

Low-Melting-Temperature Metals for Possible Use as Primary Targets at a Muon Collider Source

1 Introduction

The muons of a muon collider will arise from the decay of pions produced in the interaction of some 10^{15} protons/sec on a primary target. The associated heating of the target makes the use of a solid target problematic. Therefore liquid targets are under consideration. See sec. 4.1 of the 1996 Muon Collider Feasibility Study [1] for a general discussion of targeting issues.

While mercury or perhaps gallium suggest themselves as room-temperature liquids mercury vapor is toxic and gallium has a relatively low atomic number and correspondingly lower yield of soft pions. Furthermore, in case of an accident at the target station it would be advantageous for the target material to solidify at room temperature to aid in containment. However, the room-temperature liquid, eutectic Ga-In, may be convenient for initial studies. Small amounts of added tin and zinc reduce the melting temperature, and the cost, slightly. Reducing the amount of gallium will raise the melting temperature to above room temperature if desired, as well as increasing the average atomic number.

Some information on liquid gallium alloys can be found at
<http://www.indium.com/liquidalloys.html>

Therefore we consider here the possible use of low-melting-temperature metals, chiefly lead-bismuth alloys (variants on solders). Lead, when combined with bismuth in an alloy that is 45% Pb by weight, has a melting point of only 126°C (255°F). The Bi-Pb phase diagram is shown in Fig. 1, taken from *Alloy Phase Diagrams*, 2nd ed., Vol. III of the ASM handbook (ASM International, Materials Park, OH, 1997). [ASM stands for American Society of Metals.]

Other interesting low-melting alloys of lead and/or bismuth are made by adding cadmium, indium or tin.

Some relevant binary phase diagrams are shown in Figs. 2-10 and ternary phase diagrams are shown in Figs. 11-13.

Some quaternary and quinary alloys have extremely low melting temperature, such as alloys 117 and 136 (designated by their melting temperatures in °F). See Table 2 for a summary of physical properties of several commercial alloys.

Table 1: Properties of some elements.

Element	Atomic Number	Density (gm/cm ³)	Melting Temp. (°C)	Boiling Temp. (°C)	Heat Capacity (J/gm-°C)	Heat of Vapor. (J/gm)	Thermal Cond. (W/cm)
Bismuth	83	9.7	271	1610	0.12	501	0.079
Cadmium	48	8.6	321	767	0.23	886	0.97
Gallium	31	5.9	30	2403	0.37	3712	0.48
Indium	49	7.3	156	2073	0.23	2016	0.82
Lead	82	11.35	327	1750	0.13	858	0.35
Mercury	80	13.5	-39	357	0.14	295	0.083
Tin	50	6-7	232	2603	0.23	2487	0.67

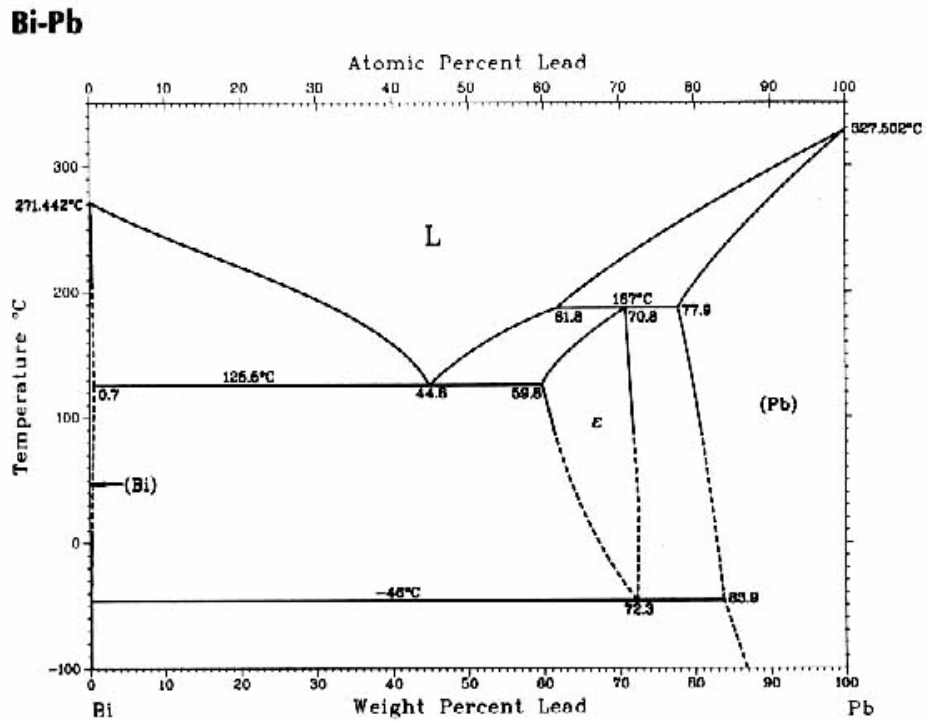


Figure 1: Bi-Pb phase diagram. Minimum melting temperature = 125.5°C.

Table 2: Alloy Specifications from Belmont Metals. See also

<http://www.indium.com/fusiblealloys.html>

TH: Kirk McDonald

Belmont
METALS INC.

330 Belmont Avenue, Brooklyn, New York 11207

(718)-342-4900 • TWX 710-584-2296 • FAX 718-342-0175

SHEET

BoB

\$96.80 \$1030

\$51.35 LB

\$13.25

\$4.95

BELMONT LOW MELTING ALLOYS - Used as Production Aids

IF
→

PHYSICAL PROPERTIES & NOMINAL COMPOSITION	EUTECTIC ALLOYS					NON EUTECTIC ALLOYS		
	BELMONT ALLOY 2451	BELMONT ALLOY 2491	BELMONT ALLOY 2505	BELMONT ALLOY 2562	BELMONT ALLOY 2581	BELMONT ALLOY 2431	BELMONT ALLOY 2481	BELMONT ALLOY 2405
Melting Temperature (°F.) Range (°F.)	117 117-117	136 136-136	158 158-158	255 255-255	281 281-281	(No definite melting point, see yield temp.) 160-190 218-440 281-338		
Yield Temp. (°F.)	117	136	158	255	281	162.5	240	302
Weight Lb./In. ³	.32	.31	.339	.380	.315	.341	.343	.296
Specific Gravity 20°C	8.9	8.8	9.4	10.3	8.7	9.4	9.5	8.2
Tensile Lb./In. ²	5400	6300	5990	6400	8000	5400	13000	8000
Elongation in 2" Slow Loading %	1.5	50	200	60-70	200	220*	Less than 1%	200*
Brinell Hardness #	12	14	9.2	10.2	22	9	19	22
*Specific Heat Liquid	.035	.032	.040	.03+	.045	.040	.045	.047
*Specific Heat Solid	.035	.032	.040	.03+	.045	.040	.045	.047
*Latent Heat — Fusion Btu./LB.	6	8	14	7.2	20	10		22
*Coefficient of Thermal Expansion	.000025/°C.	.000023/°C.	.000022/°C.	.000021/°C.	.000015/°C.	.000024/°C.	.000022/°C.	.000015/°C.
Thermal Conductivity (Solid) Cal./Cm ² /°C/Sec	—	—	*.045	*.04	*.05	*.05	—	*.09
.94 = Copper								
Conductivity (Electrical) Compared with Pure Copper	3.34%	2.43%	4.17%	1.75%	5.00%	4.27%	2.57%	7.77%
Resistivity, OHMS based on volume standard (Meter, MM ²)	.5180	.7081	.4135	.8825	.3445	.4037	.6696	.2219
*Maximum Load — 30 Seconds Lb. — In. ²			10000	8000	15000	9000	16000	15000
*Maximum Load — 5 Minutes Lb. — In. ²			4000	4000	9000	3800	10000	9500
*Safe Load — Sustained Lb. — In. ²			300	300	500	300	300	500
Volume Change (Liquid to Solid)	—1.4%	—1.35%	—1.7%	—1.5%	+0.77%	*—2.0%	—1.5%	*+0.5%
Volume Change (Linear growth after solidification.)	Less Than 0.05%	Less Than 0.05%	0.6%	0.3%	0.05%	0.3%	0.5%	*0%
GROWTH/SHRINKAGE CHARACTERISTICS TIME AFTER CASTING	FIGURES INDICATED ARE IN INCHES PER INCH AS DETERMINED FROM CUMULATIVE GROWTH MEASURED AS THE DIFFERENCE IN LENGTH BETWEEN MOLD AND TEST BAR DIMENSIONS IN A TEST BAR 1/2" x 1/2" x 10".							
2 Minutes	+0.005	+0.003	+0.025	—0.008	+0.007	—0.004	+0.008	—0.001
6 Minutes	+0.002	+0.002	+0.027	—0.011	+0.007	+0.007	+0.014	—0.001
30 Minutes	.0000	+0.001	+0.045	—0.010	+0.006	—0.009	+0.047	—0.001
1 Hour	—0.001	.0000	+0.051	—0.008	+0.006	.0000	+0.048	—0.001
2 Hours	—0.002	—0.001	+0.051	—0.004	+0.006	+0.016	+0.048	—0.001
5 Hours	—0.002	—0.002	+0.051	.0000	+0.005	+0.018	+0.049	—0.001
7 Hours	—0.002	—0.002	+0.051	+0.001	+0.005	+0.019	+0.050	—0.001
10 Hours	—0.002	—0.002	+0.051	+0.003	+0.005	+0.019	+0.050	—0.001
24 Hours	—0.002	—0.002	+0.051	+0.008	+0.005	+0.022	+0.051	—0.001
96 Hours	—0.002	—0.002	+0.053	+0.015	+0.005	+0.025	+0.055	—0.001
200 Hours	—0.002	—0.002	+0.055	+0.019	+0.005	+0.025	+0.058	—0.001
500 Hours	—0.002	—0.002	+0.057	+0.022	+0.005	+0.025	+0.061	—0.001
Compositions (%):								
Bismuth	44.7	49.0	50.0	55.5	58.0	42.5	48.0	40.0
Lead	22.6	18.0	26.7	44.5		37.7	28.5	
Tin	8.3	12.0	13.3		42.0	11.3	14.5	60.0
Cadmium	5.3		10.0			8.5		
Other	Indium 19.1	Indium 21.0					Antimony 9.0	

IF
→

* APPROXIMATE VALUES

Belmont: The Non Ferrous Specialists

—Unmatched Variety of Non Ferrous Metals and Alloys—
—Standard and Custom Compositions and Shapes—

- Casting Metals, Alloys, Additions • Joining Metals & Alloys • Low-Melting (Fusible) Alloys
- Cathodic Anodes • Plating Anodes • Wire Specialties • Chemical Metals • Mercury



Bi-Cd

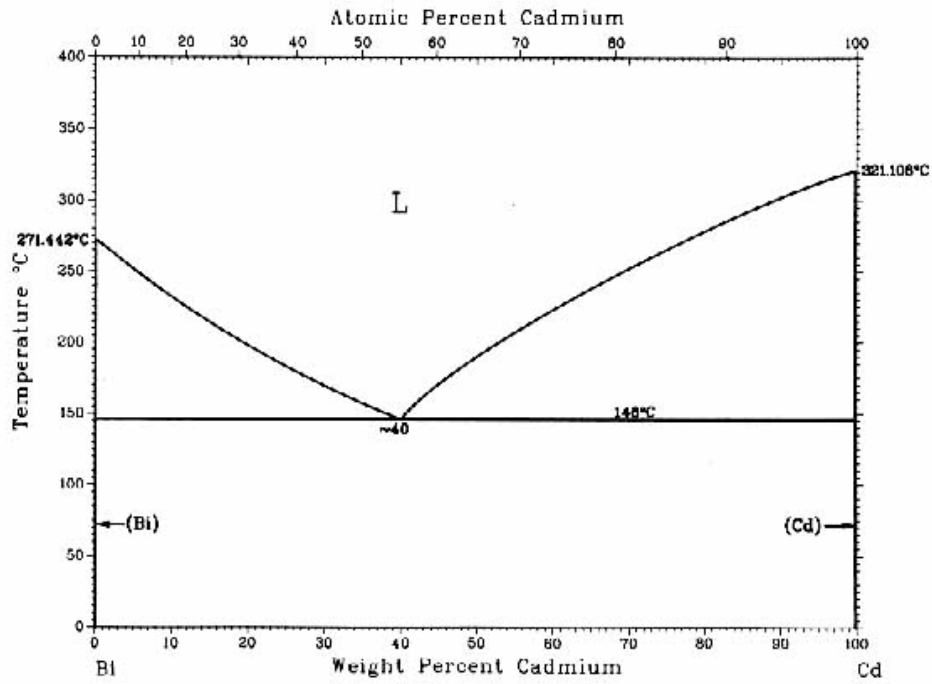


Figure 2: Bi-Cd phase diagram. Minimum melting temperature = 146°C. Cadmium vapors are somewhat toxic.

Bi-In

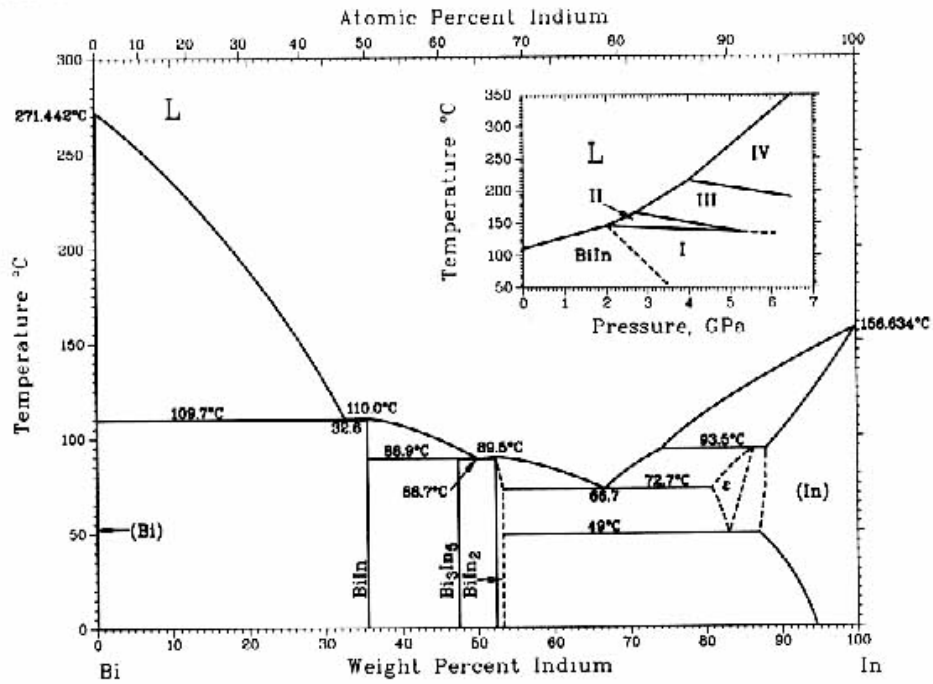


Figure 3: Bi-In phase diagram. Minimum melting temperature = 72.7°C.

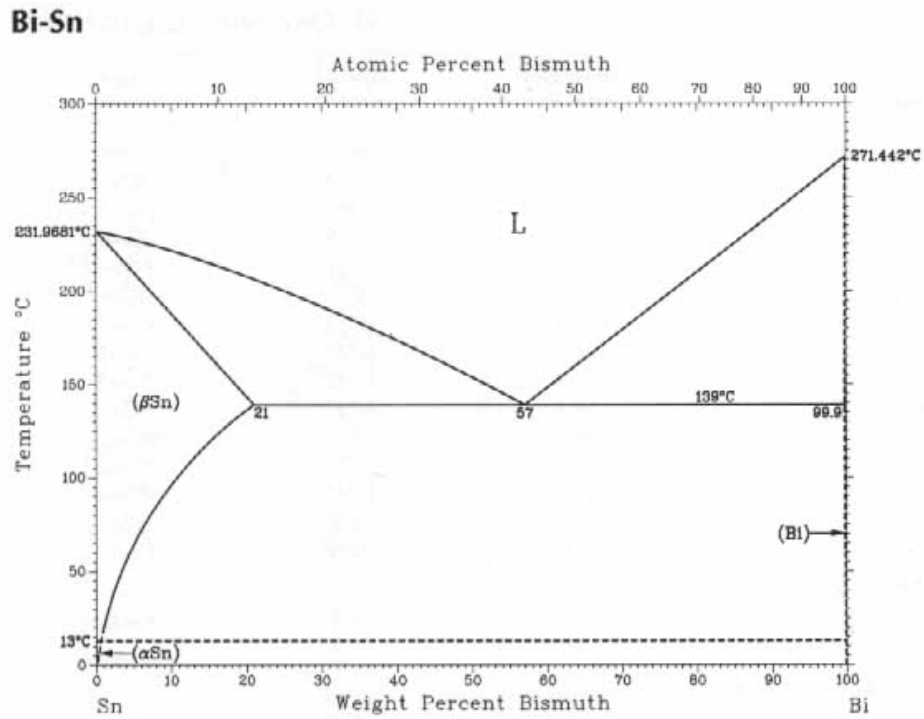


Figure 4: Bi-Sn phase diagram. Minimum melting temperature = 139°C.

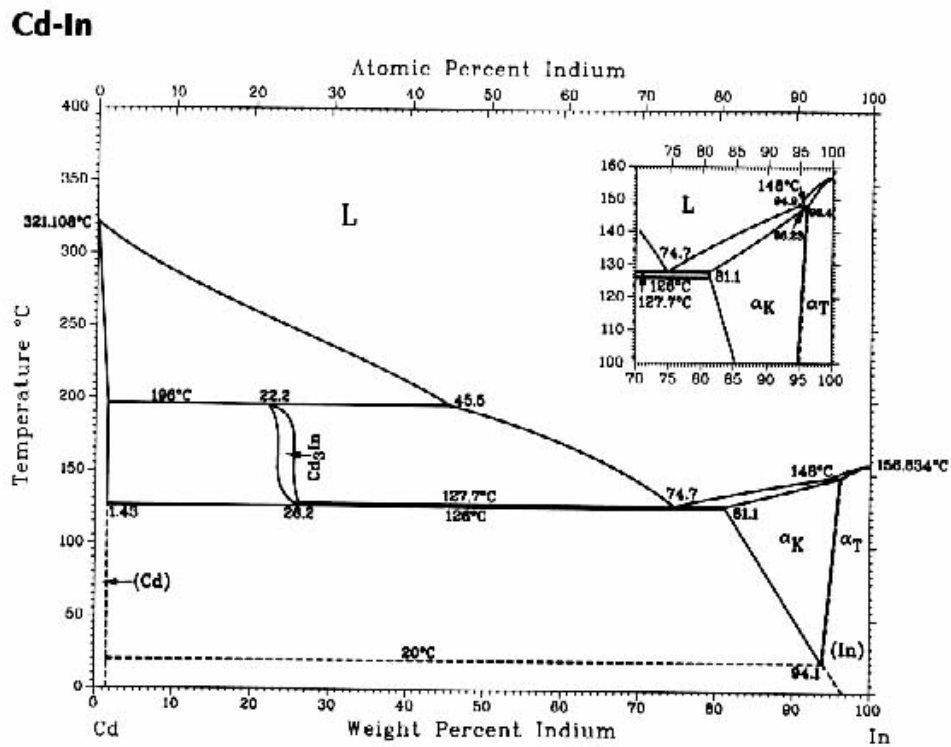


Figure 5: Cd-In phase diagram. Minimum melting temperature = 127.7°C.

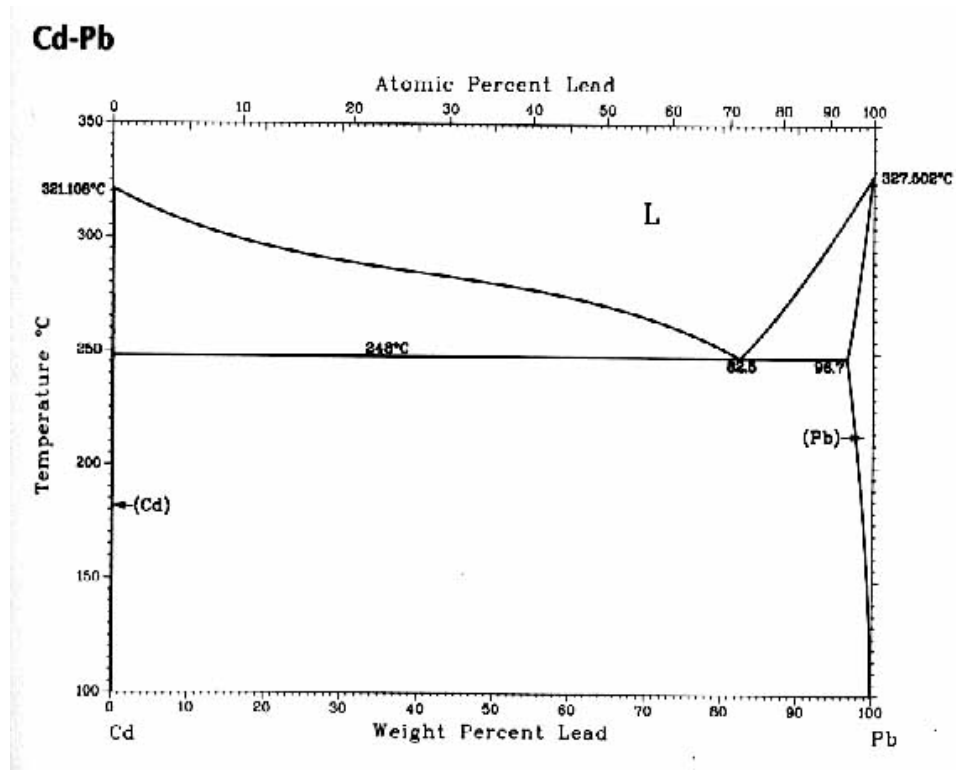


Figure 6: Cd-Pb phase diagram. Minimum melting temperature = 248°C.

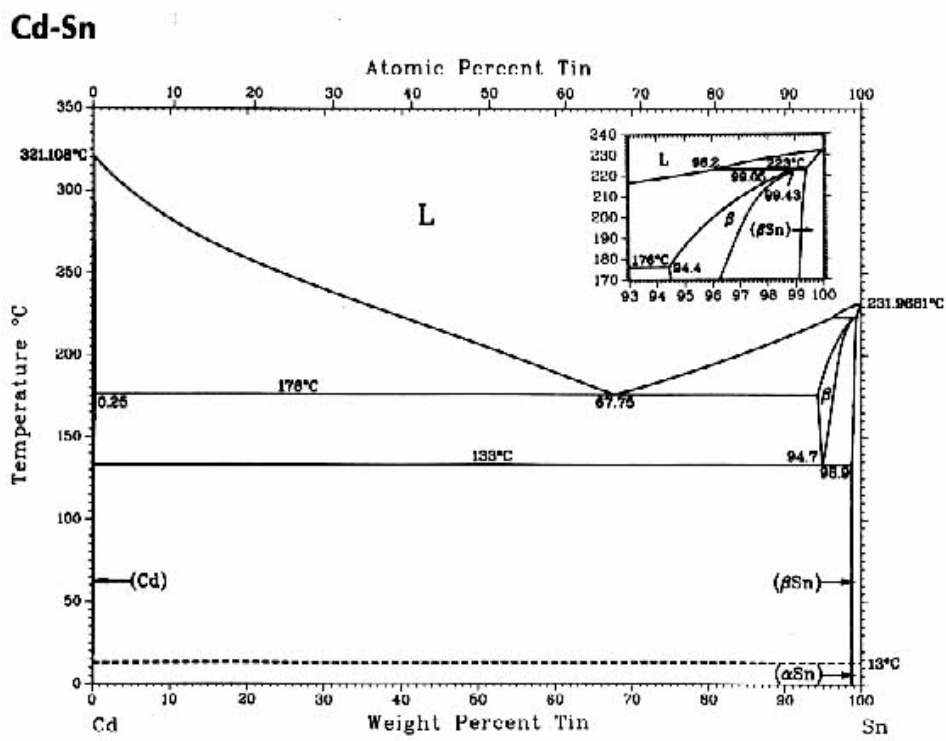


Figure 7: Cd-Sn phase diagram. Minimum melting temperature = 176°C.

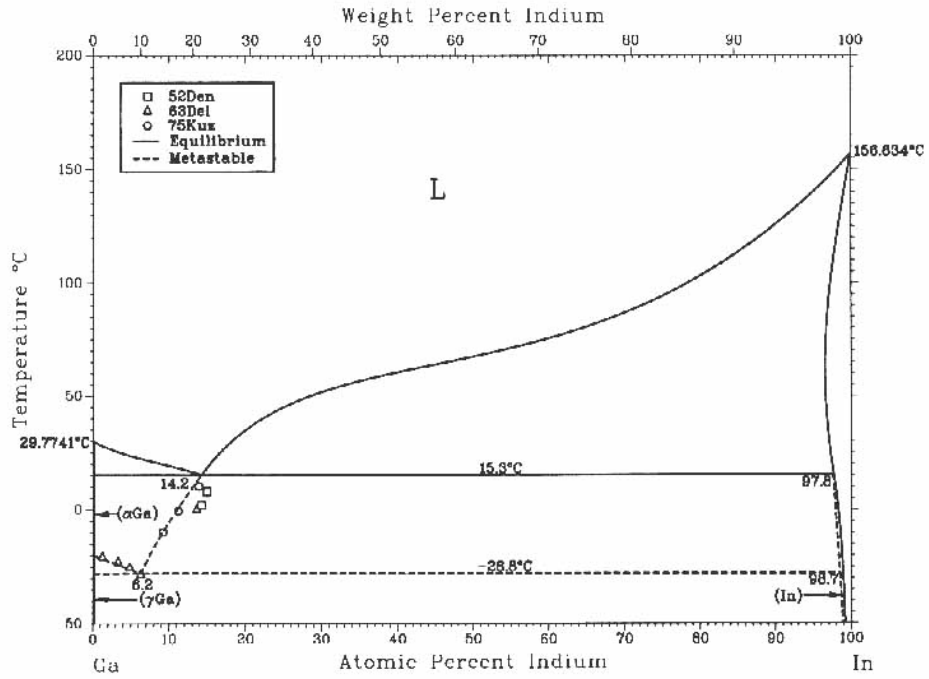


Figure 8: Ga-In phase diagram. Minimum melting temperature = 14.2°C.

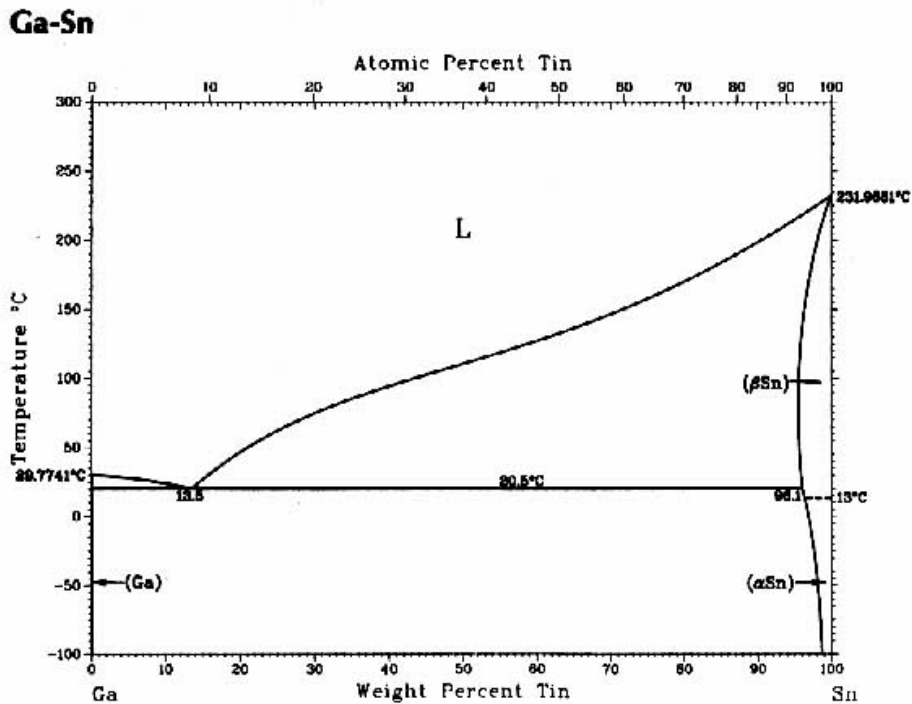


Figure 9: Ga-Sn phase diagram. Minimum melting temperature = 20.5°C.

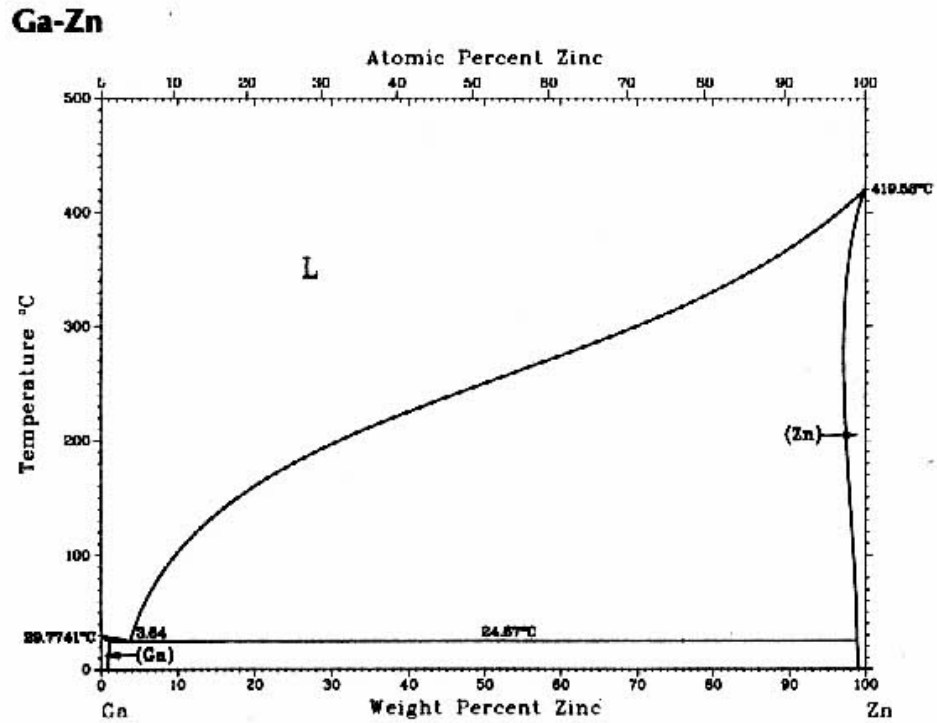


Figure 10: Ga-Zn phase diagram. Minimum melting temperature = 24.7°C.

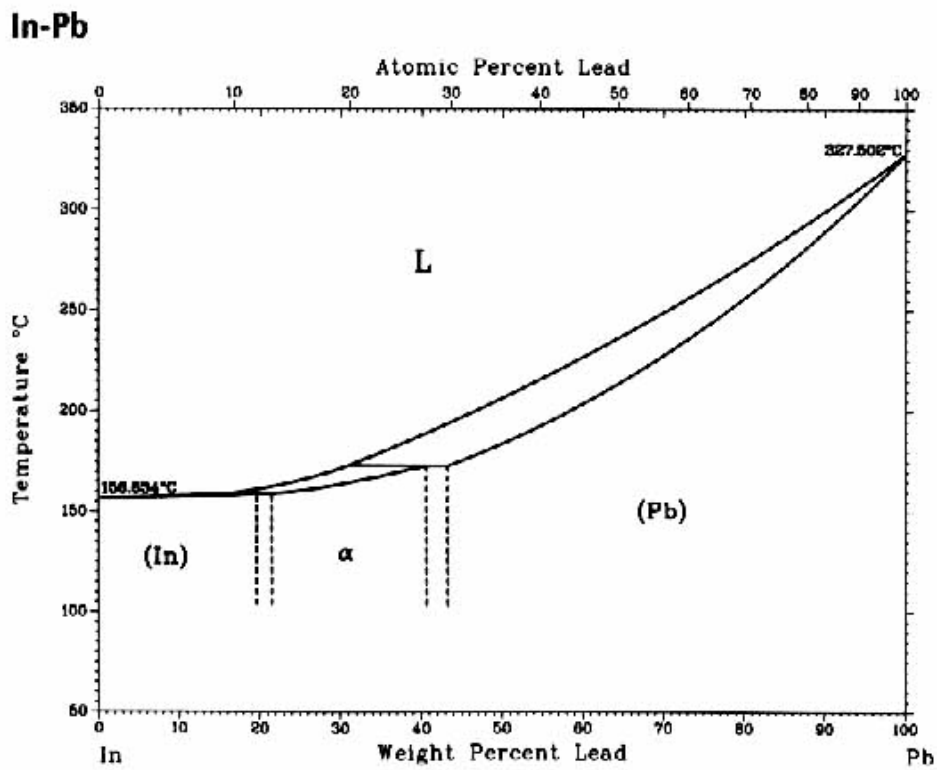


Figure 11: In-Pb phase diagram. Minimum melting temperature = 157°C.

In-Sn

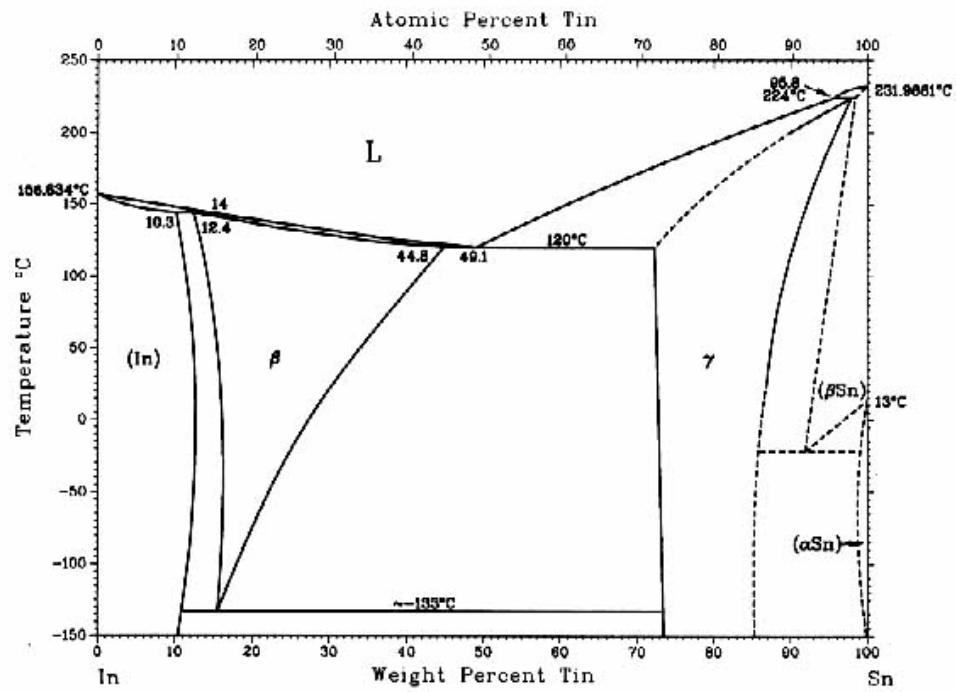


Figure 12: In-Sn phase diagram. Minimum melting temperature = 120°C.

Pb-Sn

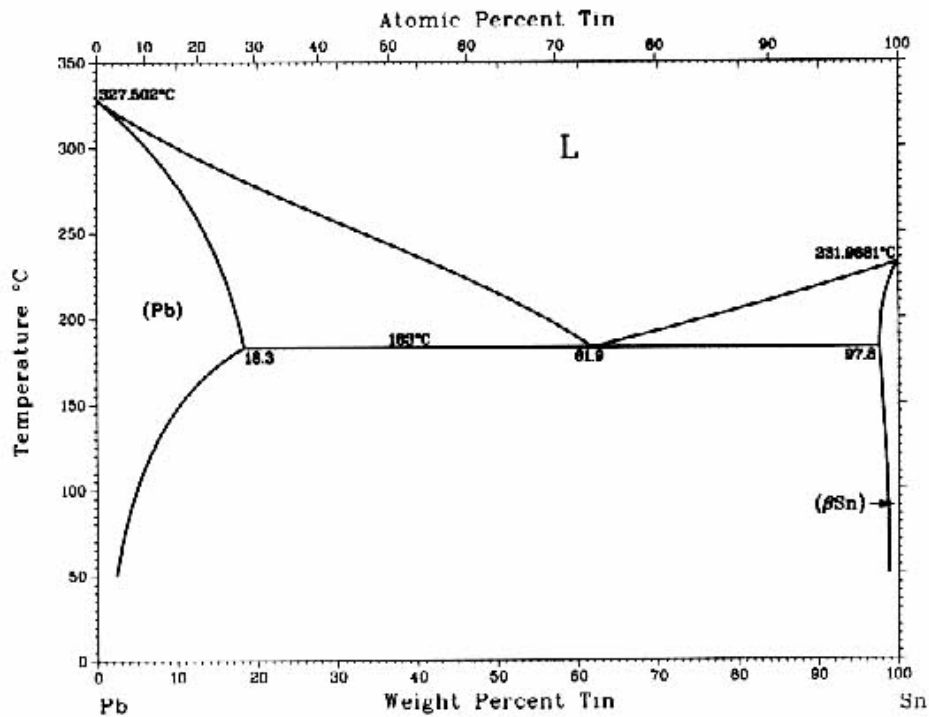


Figure 13: Pb-Sn phase diagram. Minimum melting temperature = 183°C.

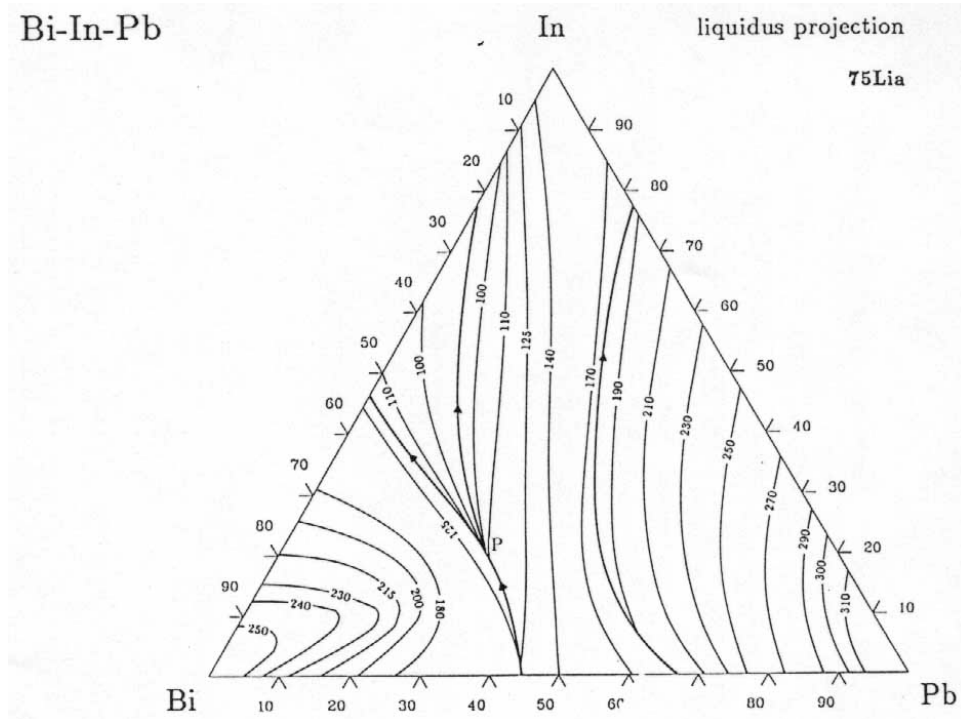


Figure 14: Bi-In-Pb phase diagram. Minimum melting temperature = 73°C.

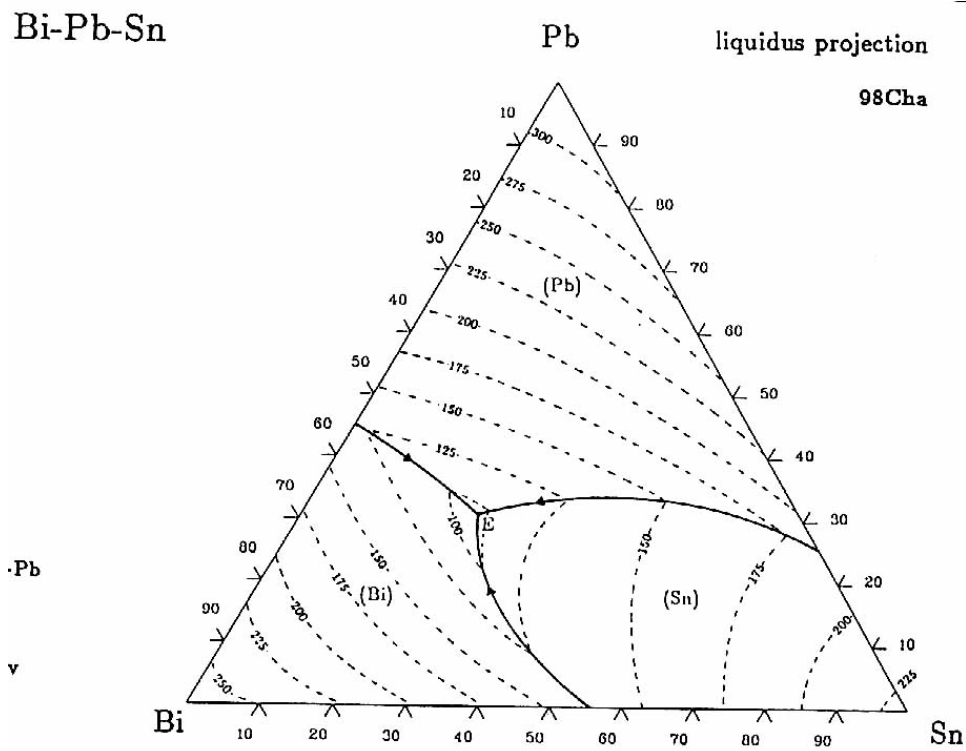


Figure 15: Bi-Pb-Sn phase diagram. Minimum melting temperature = 95°C.

2 Jet Velocity

2.1 Effect of 15-Hz Repetition Rate

We consider the use of a pulsed jet, leading to a series of cylinders of liquid, each of length l , radius r , that move with velocity v . The frequency of the pulse is f , nominally 15 Hz.

If the material from one pulse is not to overlap that of the next, then the jet velocity must obey

$$v > fl. \quad (1)$$

For example, the length of each pulse should be about two nuclear interaction lengths, or about 30 cm for a dense, high- Z material. Then with $f = 15$ Hz, we need $v > 4.5$ m/s.

The jet velocity will have to be several times this to create gaps between adjacent pulses so that the proton beam interacts only with a single jet pulse.

2.2 Effect of Gravity

The trajectory of the jet will be a parabolic arc due to the acceleration of gravity. If the jet velocity is too low, the curvature of the jet will be large, and the proton beam would not be able to intersect the jet pulse over its whole length.

The ends of the jet are displaced downward from the ideal straight trajectory by amount

$$\Delta y = \frac{gt^2}{2} = \frac{gl^2}{8v^2}, \quad (2)$$

noting that the time for the center of the jet to reach its end is $t = l/2v$. Hence, to have offset Δy between center and ends to the jet, we need

$$v = \sqrt{\frac{gl^2}{8\Delta y}}. \quad (3)$$

For example, with $l = 30$ cm, and $\Delta y = 1/8$ cm as might be desired for a jet of radius 1 cm, we find $v \approx 1000$ cm/s = 10 m/s.

Thus the effects of pulse frequency and of gravitational curvature both require the jet velocity to be at least 10 m/s.

3 Will a Strong Magnetic Field Repel a Metal Jet?

If a jet of liquid metal enters the solenoid magnet surrounding the target area it will be repelled according to Lenz' law. The effect is due to the Lorentz force on the eddy currents induced in the moving metal. In an extreme case the jet would not reach the center of the solenoid.

A good general introduction to eddy-current analysis is given §45 of *Electrodynamics of Continuous Media* by Landau and Lifshitz. §§51-55 of that book discuss the dynamics of magnetic fluids, of which the present topic is an example. Chap. 10 of *Classical Electrodynamics* by Jackson also covers magnetohydrodynamics. I have found the short book *Magnetohydrodynamics* by Cowling to be helpful also.

It is useful to establish numerical values for some relevant parameters of our system as a qualitative guide to its magnetohydrodynamic behavior.

First, we note that the problem of a moving conductor in a static magnetic field is equivalent to a moving field that encounters a conductor initially at rest. Thus, the electric field \mathbf{E}' in the frame of the conductor is related to the electric and magnetic fields \mathbf{E} and \mathbf{B} in the lab frame by

$$\mathbf{E}' = \mathbf{E} + \mathbf{v} \times \mathbf{B}, \quad (4)$$

where \mathbf{v} is the laboratory velocity of the conductor ($v \ll c$), and we use MKSA units.

Next, we recall that the penetration of a time-dependent magnetic field into a conductor is governed by a diffusion equation. Assuming $v \ll c$ and reasonably good conductivity σ , we may neglect the displacement current, and the basic electromagnetic equations are

$$\nabla \times \mathbf{E} = -\frac{\partial \mathbf{B}}{\partial t}, \quad \nabla \times \mathbf{B} = \mu_0 \mathbf{j}, \quad \text{and} \quad \mathbf{j} = \sigma \mathbf{E}' = \sigma(\mathbf{E} + \mathbf{v} \times \mathbf{B}), \quad (5)$$

where \mathbf{j} is the current density. On eliminating \mathbf{j} and \mathbf{E} we find that

$$\frac{\partial \mathbf{B}}{\partial t} = \frac{\nabla^2 \mathbf{B}}{\mu_0 \sigma} + \nabla \times (\mathbf{v} \times \mathbf{B}). \quad (6)$$

With the neglect of the second term (justified for low velocity), we find the desired diffusion equation. Thus, the characteristic time for diffusion of the magnetic field into a long conducting cylinder of radius r is

$$\tau = \mu_0 \sigma r^2. \quad (7)$$

The low-melting temperature alloys in Table 2 all have relatively low conductivity. In particular, alloy 255 has conductivity only 2% that of copper (resistivity = $1.67 \mu\Omega\text{-cm}$), *i.e.*, about 10^6 MKSA units. Hence, for a cylinder of radius 1 cm the diffusion time is

$$\tau \approx 4\pi \times 10^{-7} \cdot 10^6 (10^{-2})^2 \approx 10^{-4} \text{ sec.} \quad (8)$$

Another characteristic time in our problem is that over which the external magnetic field varies appreciably. For a jet of velocity v that enters a solenoid of diameter D , this time is D/v . The ratio of the diffusion time to time D/v is called the magnetic Reynold's number:

$$\mathcal{R} = \frac{\tau v}{D}. \quad (9)$$

For $\mathcal{R} \ll 1$ the external magnetic field penetrates the conductor, but for $\mathcal{R} \gg 1$ it does not.

Anticipating a jet velocity of order 10 m/s and a solenoid of diameter $D \approx 0.3$ m, we have $D/v \approx 0.03$ s, and the magnetic Reynold's number is $\mathcal{R} \approx 0.003$. We conclude that in our problem the diffusion is rapid enough that the external field penetrates the conductor. That is, in an important sense our candidate metals are not 'good' conductors which could exclude the magnetic field from their interior. This is fortunate, as a 'good' conductor could not enter a 20-T magnetic field unless its initial velocity were very high.¹

¹To see this, consider a good conductor moving along the z-axis of a solenoid field. Surface current $I = B_z/\mu_0$ (per unit length) is induced so as to cancel the external solenoid field B_z . This current interacts with the radial component of the external field, $B_r \approx (r/2)dB_z(0, z)/dz = rB'_z/2$ to produce retarding force $F = -2\pi rIB_r = -2\pi r(B_z/\mu_0)(rB'_z/2) = \pi r^2(B'_z)^2/2\mu_0$ per unit length. But also, $F = ma = \pi r^2 \rho \dot{v} = \pi r^2 \rho v v' = \pi r^2 \rho (v^2)'/2$, where $\rho \approx 10^4$ kg/m³ is the mass density. This integrates to give $v^2(z) = v_{-\infty}^2 - B_z^2/\mu_0 \rho$. Thus to enter a field of $B_z = 20$ T, the initial velocity would need to be at least $B_z/\sqrt{\mu_0 \rho} \approx 200$ m/s for our heavy metals.

The magnetic Reynold's number can be thought of in another way. From the point of view of the conductor, the external magnetic field is time dependent with frequency content up to $\omega \approx v/D$. The skin depth at this frequency is $\delta = \sqrt{2/\mu_0\omega\sigma} = \sqrt{2D/\mu_0\sigma v}$. This is to be compared to the radius r of the conductor. Indeed,

$$\frac{r^2}{\delta^2} = \frac{\mu_0\sigma r^2 v}{2D} = \frac{\mathcal{R}}{2}. \quad (10)$$

In our case, the low value of the magnetic Reynold's number indicates that the conductor is much smaller than the relevant skin depth, and again we expect the external field to penetrate the conductor.

We now give some approximate analyses of the forces on the liquid jet as it enters a solenoid.

3.1 Jet on Axis of a Solenoid

We model the forces on a conducting jet in a magnetic by considering only a ring (or disc) perpendicular to the axis of the jet. The ring has radius r , radial extent Δr and thickness Δz .

We first consider only motion along the axis of the ring, which we call the z axis, and which is also the axis of a solenoid magnet with field $\mathbf{B}(r, z)$.

Then the magnetic flux through the ring at position z is

$$\Phi \approx \pi r^2 B_z(0, z), \quad (11)$$

whose time rate of change is

$$\dot{\Phi} = \pi r^2 \dot{B}_z = \pi r^2 B'_z v, \quad (12)$$

where $\dot{}$ indicated differentiation with respect to time, $'$ is differentiation with respect to z , B_z stands for $B_z(0, z)$ and v is the velocity of the center of mass of the ring.

If the metal has electrical conductivity σ , then its resistance to currents around the ring is

$$R = \frac{2\pi r}{\sigma \Delta r \Delta z}, \quad (13)$$

so the (absolute value of the) induced current is

$$I = \frac{\mathcal{E}}{R} = \frac{\dot{\Phi}}{R} = \frac{\sigma r B'_z v \Delta r \Delta z}{2}. \quad (14)$$

3.1.1 Radial Pinch

The Lorentz force on the ring due to the interaction of this current with the axial field pinches the jet radially, while that due to the interaction with the radial field opposes the motion. The radial pinch can be characterized by a radial pressure gradient,

$$\frac{\Delta P_r}{\Delta r} = \frac{\Delta F_r}{\Delta r \Delta z \Delta l} = -\frac{B_z I \Delta l}{\Delta r \Delta z \Delta l} = -\frac{\sigma r B_z B'_z v}{2}. \quad (15)$$

As the jet enters the magnet from $z = -\infty$, the axial field gradient, B'_z , is initially positive, and the radial forces are inward. However, at the jet exits the solenoid, the gradient B'_z becomes negative, and the radial force is outwards. Even if the jet has not been destabilized by the pinch on entering the magnetic, the radially outward forces experienced on leaving the magnet may disperse the jet.

The pinch is greatest as the ring passes the edge of the solenoid, where $B_z \approx B_0/2$ and $B'_z \approx B_0/D$ for a solenoid of diameter D and peak axial field B_0 . That is,

$$\frac{\Delta P_{r,\max}}{\Delta r} \approx -\frac{\sigma}{4} \frac{r}{D} B_0^2 v. \quad (16)$$

Integrating this over radius, the pressure gradient between the axis and radius r is

$$\Delta P_{r,\max} \approx -\frac{\sigma}{8} \frac{r^2}{D} B_0^2 v. \quad (17)$$

3.1.2 Axial Retarding Force

The component of the Lorentz force that opposes the motion of the ring is

$$\Delta F_z = 2\pi r B_r I = -\pi \sigma r^2 B_r B'_z v \Delta r \Delta z \approx -\frac{\pi \sigma r^3 (B'_z)^2 v \Delta r \Delta z}{2}, \quad (18)$$

using the approximate relation for the radial field near the z -axis,

$$B_r(r, z) \approx -\frac{r}{2} \frac{dB_z(0, z)}{dz} = -\frac{r B'_z}{2}, \quad (19)$$

(which can be deduced from the Maxwell equation $\nabla \cdot \mathbf{B} = 0$).

The equation of motion of a ring is then

$$dF_z = -\frac{\pi \sigma r^2 (B'_z)^2 v_z \Delta z}{2} = m \dot{v}_z = 2\pi \rho r \Delta r \Delta z v'_z v_z, \quad (20)$$

where ρ is the mass density of the metal. After dividing out the common factor of $\pi r \Delta r \Delta z v_z$ we find

$$v'_z(r) = -\frac{\sigma r^2 (B'_z)^2}{4\rho}. \quad (21)$$

Before considering detailed models of the axial field profile, B_z , we note that the peak gradient of the axial field of a solenoid of diameter D is B_0/D , and the gradient is significant over a region $\Delta z \approx D$. Hence, we estimate that on entering a solenoid the jet velocity is reduced by an increment

$$\Delta v_z(r) \approx \frac{\sigma r^2 B_0^2}{4\rho D}. \quad (22)$$

On leaving the solenoid, the jet velocity is reduced by a second increment Δv_z . (Since the effect depends on $(B'_z)^2$, the sign is the same on both entering and exiting.)

The jet velocity cannot actually go negative due to the effect of the magnetic field. If the velocity reaches zero the jet stops (falls). Note that we divided eq. (20) by v_z before integrating; once v_z becomes zero F goes to zero and stays there.

The reduction of velocity is zero on axis of the jet, and grows quadratically with radius. If the jet were a rigid body, the Δv_z would be one half the value given by eq. (22) at the outer radius.

If the change in velocity is small compared to the initial velocity, $v_{-\infty}$, we estimate the distance $\Delta z(r)$ by which the material in the jet at radius r is retarded compared to the material on axis as

$$\Delta z(r) \approx \Delta v_z(r) \Delta t \approx \Delta v_z(r) \frac{D}{v_{-\infty}} \approx \frac{\sigma r^2 B_0^2}{4\rho v_{-\infty}}. \quad (23)$$

We desire this to be small compared to the length of the jet. Indeed, it will be awkward if Δ_z exceeds the radius of the jet.

We now consider more specific models.

3.1.3 Semi-Infinite Solenoid

Bob Weggel has pointed out that the fields of a semi-infinite solenoid are rather amenable to analytic calculation. Indeed, for a solenoid of radius $D/2$ with coils at $z > 0$, the axial field is

$$B_z(0, z) = \frac{B_0}{2} \left(1 + \frac{z}{\sqrt{(D/2)^2 + z^2}} \right), \quad (24)$$

whose derivative is

$$B'_z = \frac{dB_z(0, z)}{dz} = \frac{B_0}{2} \frac{(D/2)^2}{[(D/2)^2 + z^2]^{3/2}}. \quad (25)$$

Using eq. (25) in eq. (21) and integrating the equation of motion from $-\infty$ to z , we find

$$v_z(r, z) = v_{-\infty} - \frac{3\sigma r^2 B_0^2}{64\rho D} \left(\frac{\pi}{2} + \tan^{-1} w + \frac{w}{1+w^2} + \frac{2w}{3(1+w^2)^2} \right), \quad (26)$$

where D is the diameter of the solenoid and $w = 2z/D$.

The semi-infinite solenoid is meant to represent a finite solenoid of length $L = \alpha D$. Since the semi-infinite coil begins at $z = 0$, the center of the finite solenoid it approximates is at $z = \alpha D/2$, *i.e.*, at $w = \alpha$. For $\alpha \gtrsim 1$, as is reasonable for an actual magnet, there is little difference between the result of eq. (26) at $w = \alpha$ and at $+\infty$, so we estimate the change in velocity as

$$\Delta v_z(r) \approx -\frac{3\pi\sigma r^2 B_0^2}{64\rho D}. \quad (27)$$

The retardation relative to the center of the jet is related by

$$\Delta \dot{z}(r) = \Delta v_z(r) = \Delta z' v_z \approx \Delta z' v_{-\infty}, \quad (28)$$

where the approximation holds if $\Delta v_z \ll v_{-\infty}$. In this approximation, we integrate eq. (26) to find

$$\Delta z(r) \approx -\frac{3\sigma r^2 B_0^2 w}{128\rho v_{-\infty}} \left(\frac{\pi}{2} + \tan^{-1} w - \frac{1}{3w(1+w^2)} \right). \quad (29)$$

This diverges for large w , but at $w = \alpha \approx 1$, corresponding to the center of a real magnet, we have

$$\Delta z(r) \approx -\frac{3\pi\sigma r^2 B_0^2 \alpha}{128\rho v_{-\infty}}. \quad (30)$$

After a comparison with a calculation for a short solenoid, we consider numerical results in sec. 3.1.5.

3.1.4 Short Solenoid

Figure 18 shows the axial field $B_z(0, z)$ and its first derivative $dB_z(0, z)/dz$ for an idealized thin solenoid of length L and diameter D .² The derivative is approximately a Gaussian that peaks at the edge of the solenoid and has variance $D/4$:

$$\frac{dB_z(0, z)}{dz} \approx -\frac{B_0}{D} e^{-8(z-L/2)^2/D^2}. \quad (31)$$

Substituting eq. (31) for B'_z , equation (21) can be integrated to find the velocity v_0 of the ring when it reaches the center of the magnet:

$$v_0(r) = v_{-\infty} - \frac{\sqrt{\pi}\sigma r^2 B_0^2}{16\rho D}, \quad (32)$$

where $v_{-\infty}$ is the velocity of the ring at $z = -\infty$ before it enters the magnetic field.

The ring cannot penetrate into a field of strength B unless

$$v_{-\infty} > \frac{\sqrt{\pi}\sigma r^2 B_0^2}{16\rho D}. \quad (33)$$

Thus the metal ring, or jet, should have as small a radius as possible, as well as a low electrical conductivity.

Recalling the result of sec. 3.1.3, the minimum initial velocity needed for the jet to penetrate a semi-infinite solenoid is a factor of $3\sqrt{\pi}/4 = 1.33$ times larger than the corresponding velocity (33) for our model of a short solenoid. Therefore, we can use to results for a semi-infinite solenoid as a conservative estimate of those for a short solenoid.

²For the record, the axial field is given in problem 5.2 of Jackson as $B_z = B_0(\cos\theta_1 + \cos\theta_2)\sqrt{1 + D^2/L^2}/2$, which translates to

$$B_z(0, z) = \frac{B_0}{2} \left(\frac{1 + 2z/L}{\sqrt{1 + 4(z/L)(z/L + 1)/(1 + D^2/L^2)}} + \frac{1 - 2z/L}{\sqrt{1 + 4(z/L)(z/L - 1)/(1 + D^2/L^2)}} \right),$$

and

$$\frac{dB_z}{dz} = \frac{B_0}{D} \frac{D^3/L^3}{1 + D^2/L^2} \left(\frac{1}{[1 + 4(z/L)(z/L + 1)/(1 + D^2/L^2)]^{3/2}} - \frac{1}{[1 + 4(z/L)(z/L - 1)/(1 + D^2/L^2)]^{3/2}} \right).$$

The origin is at the center of the solenoid.

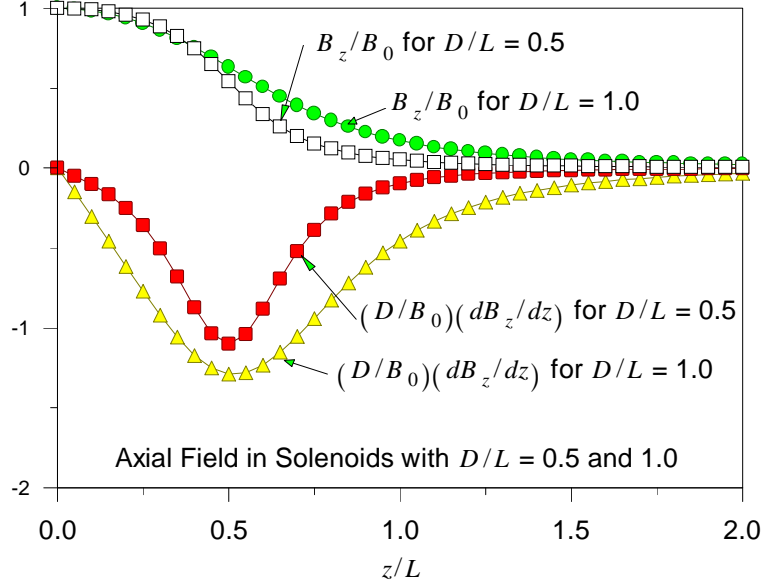


Figure 18: The axial field $B_z(0, z)$ and its first derivative $dB_z(0, z)/dz$ in an ideal thin solenoid of length L and diameter D for the two cases $D/L = 0.5$ and 1.0 .

3.1.5 Numerical Examples

The low-melting temperature alloys in Table 2 all have relatively low conductivity. In particular, alloy 255 has conductivity only 2% that of copper (resistivity = $1.67 \mu\Omega\text{-cm}$), *i.e.*, about 10^6 MKSA units. The density of alloy 255 is about 10 gm/cm^3 , *i.e.*, 10^4 kg/m^3 . Then, eq. (27) leads to the requirement

$$v_{-\infty} > 60 \text{ m/s} \left[\frac{r}{1 \text{ cm}} \right] \left[\frac{r}{D} \right] \left[\frac{B_0}{20 \text{ T}} \right]^2. \quad (34)$$

It is thought that the jet radius must be 0.5-1 cm to match the proton beam, and that the inside diameter of the solenoid will be about 20 cm. In this case we need $v_{-\infty} > 0.75\text{-}3 \text{ m/s}$ for $B_0 = 20 \text{ T}$.

Again, if the jet is to exit the magnet, $v_{-\infty}$ must be twice the minimum given in (34).

In the approximation of eq. (30), the shear in the jet profile between its axis and radius r is

$$\frac{\Delta z(r)}{r} \approx -3\alpha \left[\frac{r}{1 \text{ cm}} \right] \left[\frac{B_0}{20 \text{ T}} \right]^2 \left[\frac{10 \text{ m/s}}{v_{-\infty}} \right]. \quad (35)$$

For, say, $r = 1 \text{ cm}$, $v_{-\infty} = 10 \text{ m/s}$, $\alpha = 2$ and $B_0 = 20 \text{ T}$, we would have $\Delta z(r) \approx 6r$, which is a fairly severe distortion of the jet.

Returning to the issue of the radial pinch, we can now cast eq. (17) in the form

$$\Delta P_{r,\text{max}} \approx 50 \text{ atm.} \left[\frac{r}{1 \text{ cm}} \right] \left[\frac{r}{D} \right] \left[\frac{B_0}{20 \text{ T}} \right]^2 \left[\frac{v_{-\infty}}{10 \text{ m/s}} \right]. \quad (36)$$

For, say, $r = 1$ cm, $v_{-\infty} = 10$ m/s, $D = 20$ cm and $B_0 = 20$ T, the maximum radial pressure is 2.5 atmosphere. While not large, this may still be enough to perturb the shape of the jet as it enters the magnet.

When the jet leaves the magnet, the radial pressure goes negative. This pressure is still small compared to the tensile strength of the jet material, so the jet will not necessarily tear apart. However, the rapid change of pressure from positive to negative may excite oscillations of the jet which lead to breakup into macroscopic droplets. This would occur after the proton beam interacted with the jet, so is more of a nuisance for the liquid collection system than a fundamental flaw.

The longitudinal effects, (34) and (35), are suppressed at higher jet velocities, which, however, enhances the radial pinch (36).

3.2 Jet at an Angle to the Axis of a Solenoid

To improve the yield of pions in the interaction of the proton beam with the liquid jet, it is desirable that the jet axis make a small angle $\theta \approx 0.1$ to the axis of the solenoid. In this case the motion of the jet includes a component at right angles to the magnetic field.

3.2.1 Magnetic Viscosity

We first make some general observations, following p. 10 of the book by Cowling. We suppose that the liquid is incompressible, so that the distribution of velocities with the jet obeys $\nabla \cdot \mathbf{v} = 0$. The equation of motion for the fluid is

$$\rho \frac{d\mathbf{v}}{dt} = -\nabla P + \rho \mathbf{g} + \eta \nabla^2 \mathbf{v} + \mathbf{j} \times \mathbf{B}, \quad (37)$$

where ρ is the mass density, P is the pressure, \mathbf{g} is the acceleration due to gravity and η is the viscosity of the liquid. The current density \mathbf{j} is related to the electric and magnetic fields according to eq. (5), so the electromagnetic part of the equation of motion can be written

$$\rho \frac{d\mathbf{v}}{dt} = \sigma(\mathbf{E} + \mathbf{v} \times \mathbf{B}) \times \mathbf{B} = \sigma(\mathbf{E}_{\perp} \times \mathbf{B} - B^2 \mathbf{v}_{\perp}), \quad (38)$$

where \mathbf{E}_{\perp} and \mathbf{v}_{\perp} are the components of those vectors that are perpendicular to the magnetic field \mathbf{B} . If the induced electric fields, \mathbf{E} , are small compared to the magnetic fields (but see below), the \perp component of eq. (38) has the form of the diffusion equation;

$$\left. \frac{d\mathbf{v}}{dt} \right|_{\perp} \approx \frac{d\mathbf{v}_{\perp}}{dt} \approx -\frac{\sigma B^2 \mathbf{v}_{\perp}}{\rho}. \quad (39)$$

The minus sign indicates that v_{\perp} decays rather than grows. The characteristic decay time is

$$\tau_{\perp} = \frac{\rho}{\sigma B^2} \approx \frac{10^4}{10^6(20)^2} = 2.5 \times 10^{-5} \text{ s} \quad (40)$$

for alloy 255 in a 20-T magnetic field. This time is short compared to the time $D/v \approx 0.3/10 = 0.03$ s for the jet to enter the solenoid. This suggests that transverse electromagnetic

forces will arise that are strong enough that the jet enters the solenoid along a magnetic field line. If so, when the jet reaches the center of the solenoid it will be aligned along the axis of the solenoid.

The resistance of the liquid to crossing field lines has been called ‘magnetic viscosity’ by Chandrasekhar.

The preceding conclusions are consistent with a qualitative interpretation of the radial forces considered in sec. 3.1.1. That is, motion along the field lines of a solenoid requires radially inward forces on entering the solenoid, but radially outwards forces on exiting.

In the preceding we ignored the effect of ordinary viscosity η , whose value we estimate to be 0.001 MKS units, this being the viscosity of mercury. To assess the validity of this assumption, we note that the volume force associated with ‘magnetic viscosity’ is $\sigma B^2 v_\perp$, while that associated with ordinary viscosity is $\eta v_\perp / r^2$ (for a jet roughly aligned with the solenoid axis). The square root of the ratio of these volume forces is called the ‘Hartmann number’ M :

$$M = rB\sqrt{\frac{\sigma}{\eta}} \approx 0.01 \cdot 20\sqrt{\frac{10^6}{10^{-3}}} \approx 6 \times 10^3. \quad (41)$$

Since $M \gg 1$, we infer that magnetic viscosity is indeed much more important than ordinary viscosity in our case.

However, we have also neglected the transverse components of ∇P and \mathbf{E} in the preceding. Particularly in the case of the electric field, this may not be a good approximation. Let us review the derivation of eq. (39) from a simple point of view. It indicates that a retarding force should arise even for motion of a conductor at right angles to a uniform magnetic field. First, the $\mathbf{v} \times \mathbf{B}$ force on the conduction electrons results in a current density $\mathbf{j} = \sigma \mathbf{v} \times \mathbf{B}$, if there is no opposing electric field. This current is also perpendicular to the magnetic field, so the volume force density on this current is $\mathbf{j} \times \mathbf{B}$, which leads to eq. (39).

But, does the current, $\mathbf{j} = \sigma \mathbf{v} \times \mathbf{B}$, persist? This current leads to charge separation, which leads to an electric field directed opposite to \mathbf{j} , which tends to cancel the $\mathbf{v} \times \mathbf{B}$ force. Thus the current most likely exists only for a short time. Indeed, we expect that the charges will rearrange themselves within the conductor on times of order $\sigma/\epsilon_0 \approx 10^{-18}$ s to cancel out any ‘static’ field inside the conductor, such as the field $\mathbf{v} \times \mathbf{B}$. It seems that situations in which ‘magnetic viscosity’ is important are more subtle than simple uniform motion of a conductor perpendicular to a magnetic field.

We are left with the qualitative prediction that the trajectory of the jet will tend follow the magnetic field lines in a nonuniform field, but there is some doubt as to the quantitative aspect of this statement.

3.2.2 Simple Model of Motion in Nonuniform Magnetic Field

(This section follows a note by Bob Weggel dated Dec. 11, 1997 [2]. The method introduced in this section is applied in the following section to the problem of a conducting jet moving through a solenoid.)

If the magnetic field is nonuniform, eddy currents arise that lead to forces which oppose motion at right angles to the magnetic field lines.

For a simple calculation, we consider a magnetic field whose main component is in the z direction, but whose strength is a function of x : $B_z = B_z(x)$. A conductor moves with

velocity v_x in the x direction through this magnetic field; *i.e.*, the motion is at right angles to the field lines.

We suppose that a static field, $\mathbf{E}_{\text{static}}$ arises that exactly cancels the $\mathbf{v} \times \mathbf{B}$ force (which is in the y direction); *i.e.*, $\mathbf{E}_{\text{static}} + \mathbf{v} \times \mathbf{B} = 0$.

However, because the field is nonuniform, the flux varies through any loop inside the moving conductor that lies in the x - y plane. Thus an eddy current, \mathbf{j} , flows in the x - y plane. The $\mathbf{j} \times \mathbf{B}$ force on the eddy current has a component that opposes the velocity v_x that induces it. In particular, we need to calculate the y component of the eddy current.

To analyze the eddy currents we make an assumption that they flow in concentric loops about the center of symmetry of the conductor in the x - y plane. For a simple model, we take the conductor to be rectangular with extent $\Delta x \times \Delta y \times \Delta z$, and analyze the problem at the moment that the center of the conductor is at the origin.

The eddy currents then flow in loops (tubes) of cross section $\epsilon \Delta x \times \epsilon \Delta y$, where $0 \leq \epsilon \leq 1$. The flux through the loop of parameter ϵ is

$$\Phi \approx \epsilon^2 B_z(0) \Delta x \Delta y, \quad (42)$$

supposing the field does not vary too much over distance Δx . The emf \mathcal{E} induced around this loop is therefore

$$\mathcal{E} = -\dot{\Phi} = -v_x \Phi_{,x} = -v_x \epsilon^2 B_{z,x} \Delta x \Delta y, \quad (43)$$

noting that the motion of the conductor in x causes the change in the linked flux; the subscript $,x$ indicates differentiation with respect to x .

The emf induces a current I around the loop, which extends from ϵ to $\epsilon + \Delta\epsilon$. The area element perpendicular to the current is then $\Delta\epsilon \Delta y \Delta z / 2$ for that part of the loop parallel to the x axis, and $\Delta\epsilon \Delta x \Delta z / 2$ for that part of the loop parallel to the y axis. The corresponding electric fields are then

$$E_x = \frac{j_x}{\sigma} = \frac{2I}{\sigma \Delta\epsilon \Delta y \Delta z}, \quad \text{and} \quad E_y = \frac{2I}{\sigma \Delta\epsilon \Delta x \Delta z}. \quad (44)$$

The emf equals the line integral of the electric field around the loop:

$$\mathcal{E} = 2(E_x \epsilon \Delta x + E_y \epsilon \Delta y) = \frac{4\epsilon I}{\sigma \Delta\epsilon \Delta z} \left(\frac{\Delta x}{\Delta y} + \frac{\Delta y}{\Delta x} \right), \quad (45)$$

and hence,

$$I = \frac{\sigma \Delta\epsilon \Delta z}{4\epsilon \left(\frac{\Delta x}{\Delta y} + \frac{\Delta y}{\Delta x} \right)} \mathcal{E} = -\frac{v_x \sigma \epsilon \Delta\epsilon B_{z,x} \Delta x \Delta y \Delta z}{4 \left(\frac{\Delta x}{\Delta y} + \frac{\Delta y}{\Delta x} \right)} = -\frac{v_x \sigma \epsilon \Delta\epsilon B_{z,x} V}{4 \left(\frac{\Delta x}{\Delta y} + \frac{\Delta y}{\Delta x} \right)}, \quad (46)$$

where V is the total volume of the conductor.

The x component of the $\mathbf{I} \times \mathbf{B}$ force on the current loop is due to the y currents at $\pm \epsilon \Delta x / 2$:

$$dF_x = -\frac{v_x \sigma \epsilon \Delta\epsilon B_{z,x} V}{4 \left(\frac{\Delta x}{\Delta y} + \frac{\Delta y}{\Delta x} \right)} \epsilon \Delta y [B_z(\epsilon \Delta x / 2) - B_z(-\epsilon \Delta x / 2)] = -\frac{v_x \sigma \epsilon^3 \Delta\epsilon (B_{z,x})^2 \Delta x \Delta y V}{4 \left(\frac{\Delta x}{\Delta y} + \frac{\Delta y}{\Delta x} \right)}, \quad (47)$$

ignoring higher-order field derivatives. The total retarding force on the conductor is obtained by integrating over ϵ from 0 to 1:

$$F_x = -\frac{v_x \sigma (B_{z,x})^2 \Delta x \Delta y V}{16 \left(\frac{\Delta x}{\Delta y} + \frac{\Delta y}{\Delta x} \right)}. \quad (48)$$

The x component of the equation of motion is then

$$F_x = m \dot{v}_x = \rho V v_x v_{x,x} = -\frac{v_x \sigma (B_{z,x})^2 \Delta x \Delta y V}{16 \left(\frac{\Delta x}{\Delta y} + \frac{\Delta y}{\Delta x} \right)}, \quad (49)$$

so that

$$v_{x,x} = -\frac{\sigma (B_{z,x})^2 \Delta x \Delta y}{16 \rho \left(\frac{\Delta x}{\Delta y} + \frac{\Delta y}{\Delta x} \right)}, \quad (50)$$

The case of motion in the x - z plane, rather than simply along the x axis, is taken up in the following section.

3.2.3 Motion at Angle θ to the Axis of a Solenoid

In this section we continue the argument of the preceding section. But here we consider a conducting cylinder of radius a , moving with its axis at angle θ to the axis of a solenoid magnet.

Induced Current in a Disc. The induced eddy currents will flow in loops that are roughly perpendicular to the magnetic field lines. As a simplification, we suppose that the current loops are circles perpendicular to the axis of the solenoid. This approximation should be reasonable for small θ .

The (unperturbed) trajectory of the conductor is taken to be along the line

$$x = z\theta, \quad (51)$$

where z increases with increasing time. To simplify the calculations, we suppose the trajectory follows eq. (51) even though the velocity of the jet is perturbed by the magnetic field (impulse approximation).

The radius of a current loop is ϵa , with $0 \leq \epsilon \leq 1$. The flux through a loop is

$$\Phi \approx \pi \epsilon^2 a^2 B_z(x = z\theta, z). \quad (52)$$

supposing the magnetic field does not vary too rapidly over the loop.

The axial component of a circularly symmetric magnetic field can be expanded as

$$B_z(r, z) = B_z(0, z) - \frac{r^2}{4} \frac{d^2 B_z(0, z)}{dz^2} + \dots \equiv B_z - \frac{r^2}{4} B_z'' + \dots, \quad (53)$$

where the symbol $'$ indicates differentiation with respect to z . In eq. (52) it suffices to approximate $B_z(x, z)$ by the field on the axis, which we call B_z .

The emf \mathcal{E} induced around the loop due to its motion is then

$$\mathcal{E} = -\dot{\Phi} = -(\mathbf{v} \cdot \nabla)\Phi \approx -v_z \Phi' \approx -\pi \epsilon^2 a^2 v_z B'_z. \quad (54)$$

The resistance of a conducting loop that extends in radius from ϵ to $\epsilon + \Delta\epsilon$ and has thickness Δz is

$$R = \frac{2\pi\epsilon a}{\sigma\Delta\epsilon a\Delta z} = \frac{2\pi\epsilon}{\sigma\Delta\epsilon\Delta z}. \quad (55)$$

Hence, the current I induced in this loop is

$$I = \frac{\mathcal{E}}{R} = -\frac{\sigma a^2 v_z B'_z \epsilon \Delta\epsilon \Delta z}{2}. \quad (56)$$

Force on the Disc. We next calculate the force on the loop according to

$$\mathbf{F} = \int I d\mathbf{l} \times \mathbf{B}. \quad (57)$$

The loop lies in the x - y plane with its center at $(x, y, z) = (z\theta, 0, z)$. We label the azimuth of a point on the loop by angle ϕ with respect to the x axis. Then the (x, y, z) coordinates of the point are

$$(z\theta + \epsilon a \cos \phi, \epsilon a \sin \phi, z). \quad (58)$$

The distance r between the point and the z axis is

$$r = \sqrt{(z\theta)^2 + (\epsilon a)^2 + 2\epsilon a z\theta \cos \phi}. \quad (59)$$

The line element on the loop of radius ϵa is

$$d\mathbf{l} = \epsilon a d\phi (-\sin \phi, \cos \phi, 0). \quad (60)$$

The magnetic field at the loop is

$$\begin{aligned} \mathbf{B} &= (B_x, B_y, B_z) = \left(B_r(r, z) \frac{z\theta + \epsilon a \cos \phi}{r}, B_r(r, z) \frac{\epsilon a \sin \phi}{r}, B_z(r, z) \right) \\ &\approx \left(-B'_z \frac{z\theta + \epsilon a \cos \phi}{2}, -B'_z \frac{\epsilon a \sin \phi}{2}, B_z - \frac{(z\theta)^2 + (\epsilon a)^2 + 2\epsilon a z\theta \cos \phi}{4} B''_z \right), \end{aligned} \quad (61)$$

using eqs. (19) and (53). The force element is then

$$\begin{aligned} d\mathbf{F} &= I d\mathbf{l} \times \mathbf{B} = I \epsilon a d\phi \left[\hat{\rho} B_z(r, z) + \hat{\mathbf{z}} \frac{B'_z}{2} (\epsilon a + z\theta \cos \phi) \right]. \\ &= I \epsilon a d\phi \left[(\hat{\mathbf{x}} \cos \phi + \hat{\mathbf{y}} \sin \phi) \left(B_z - \frac{(z\theta)^2 + (\epsilon a)^2 + 2\epsilon a z\theta \cos \phi}{4} B''_z \right) + \hat{\mathbf{z}} \frac{B'_z}{2} (\epsilon a + z\theta \cos \phi) \right], \end{aligned} \quad (62)$$

where $\hat{\rho}$ is the unit vector pointing radially outwards from the axis of the jet ($\rho = \epsilon a$).

The transverse force can be decomposed into a radial pinch (or expansion) as discussed in sec. 3.1 plus a drag in the x direction. The longitudinal (z) force vanishes on the axis of the jet, has a drag that is independent of azimuth, and another component that varies with azimuth causing a torque (or shear).

Drag Forces. We first ignore the radial pinch and the shear by integrating eq. (63 over ϕ and using eq. (56) for I to obtain

$$d\mathbf{F} = \frac{\pi\sigma a^4 v_z B'_z \epsilon^3 \Delta \epsilon \Delta z}{2} \left(\hat{\mathbf{x}} \frac{z\theta B''_z}{2} - \hat{\mathbf{z}} B'_z \right). \quad (63)$$

The z component of the drag force is the same as found previously in eq. (18). The retarding force vanishes on the jet axis, and increases as the cube of the radius within the jet. As a result, the core of the jet will move ahead of the outer regions.

In turn, we integrate this over ϵ to obtain the total force on a disc³ of thickness Δz :

$$\mathbf{F} = \frac{\pi\sigma a^4 v_z B'_z \Delta z}{8} \left(\hat{\mathbf{x}} \frac{z\theta B''_z}{2} - \hat{\mathbf{z}} B'_z \right). \quad (64)$$

In the equation of motion, we again replace differentiation by time with that by z :

$$\mathbf{F} = m\dot{\mathbf{v}} = \pi a^2 \Delta z \rho v_z \mathbf{v}'. \quad (65)$$

The components of the equation of motion of the conducting jet are thus,

$$v'_x = \frac{\sigma a^2 z \theta B'_z B''_z}{16\rho}, \quad \text{and} \quad v'_z = -\frac{\sigma a^2 (B'_z)^2}{8\rho}. \quad (66)$$

We will use the example of a semi-infinite solenoid to illustrate the effect of the eddy currents on the jet velocity, because the needed field derivatives have simple analytic forms. The form of the trajectory, (51), assumes that the center of the magnet is at the origin. Suppose the length of the physical magnet is α times its diameter D , so that the coil extends over $-\alpha D/2 \leq z \leq \alpha D/2$. Then the field of the physical magnet can be represented by the field of a semi-infinite solenoid whose coil begins at $z = -\alpha D/2$. Comparing with sec. 3.1.3, the field derivatives are

$$B_z = B_z(0, z) = \frac{B_0}{2} \left(1 + \frac{z + \alpha D/2}{\sqrt{(D/2)^2 + (z + \alpha D/2)^2}} \right) = \frac{B_0}{2} \left(1 + \frac{w}{\sqrt{1 + w^2}} \right), \quad (67)$$

$$B'_z = \frac{dB_z(0, z)}{dz} = \frac{B_0}{2} \frac{(D/2)^2}{[(D/2)^2 + (z + \alpha D/2)^2]^{3/2}} = \frac{B_0}{D} \frac{1}{(1 + w^2)^{3/2}}, \quad (68)$$

and

$$B''_z = \frac{d^2 B_z(0, z)}{dz^2} = -\frac{3B_0}{2} \frac{(D/2)^2 (z + \alpha D/2)}{[(D/2)^2 + (z + \alpha D/2)^2]^{5/2}} = -\frac{6B_0}{D^2} \frac{w}{(1 + w^2)^{5/2}}, \quad (69)$$

where $w = 2z/D + \alpha$.

Inserting (67-69) into (66), we see that v'_z is always negative but that v'_x is negative only until the jet enters the magnet ($z = -\alpha D/2$). Integrating (66) from $-\infty$ to z , we find that the velocity components of the jet are

$$v_x = v_{x, -\infty} - \frac{3\sigma a^2 B_0^2 \theta}{1024\rho D} \left[\frac{\pi}{2} + \tan^{-1} w + \frac{w}{1 + w^2} + \frac{2w}{3(1 + w^2)^2} - \frac{16z}{3D(1 + w^2)^3} \right], \quad (70)$$

³If we desire a calculation for a sphere rather than a disc, Δz times the integration over ϵ becomes $2a \int_0^1 \epsilon^3 \sqrt{1 - \epsilon^2} d\epsilon = 4a/15$, so $F_z = -2\pi\sigma a^5 v_z (B'_z)^2/15$. See also [3]

and

$$v_z = v_{z,-\infty} - \frac{3\sigma a^2 B_0^2}{128\rho D} \left[\frac{\pi}{2} + \tan^{-1} w + \frac{w}{1+w^2} + \frac{2w}{3(1+w^2)^2} \right]. \quad (71)$$

Of course, $v_{x,-\infty} = \theta v_{z,-\infty}$ by assumption. The velocity components of the jet when it reaches the center of the magnet ($z = 0$, $w = \alpha$) are

$$v_{x,0} = \theta v_{z,-\infty} - \frac{3\sigma a^2 B_0^2 \theta}{1024\rho D} \left[\frac{\pi}{2} + \tan^{-1} \alpha + \frac{\alpha}{1+\alpha^2} + \frac{2\alpha}{3(1+\alpha^2)^2} \right], \quad (72)$$

and

$$v_{z,0} = v_{z,-\infty} - \frac{3\sigma a^2 B_0^2}{128\rho D} \left[\frac{\pi}{2} + \tan^{-1} \alpha + \frac{\alpha}{1+\alpha^2} + \frac{2\alpha}{3(1+\alpha^2)^2} \right], \quad (73)$$

Thus, while both v_x and v_z are reduced on entering the solenoid, the relative reduction in the x velocity is only 1/8 that of the z velocity. As a consequence, the angle θ of the trajectory to the axis of the solenoid actually increases as the jet enters the magnet. For example, suppose that $v_{z,-\infty}$ is 3 times the loss of velocity on entering the magnet. Then

$$v_{z,0} = \frac{2}{3}v_{z,-\infty}, \quad v_{x,0} = \frac{23}{24}\theta v_{z,-\infty}, \quad (74)$$

and the angle of the trajectory at the center of the magnet is

$$\theta_0 = \frac{v_{x,0}}{v_{z,0}} = \frac{69}{48}\theta = 1.44\theta. \quad (75)$$

Figure 19 illustrates the variation of v_x , v_z and θ of the jet as a function of z .

We are greatly encouraged by these idealized calculations that the effect of eddy currents on the transverse velocity of the jet will not be too severe.

The above analysis is only for the drag force on the jet as a whole. Recall that the force varies with radius within the jet, and so leads to longitudinal distortions as discussed in sec. 3.1. The variation of the drag force in x leads to additional torques and shears, which we now discuss.

Torque and Shear. The magnetic forces on the eddy currents also produce a torque that will twist the jet about the axis perpendicular to the plane of the jet motion – the y axis in our example.

The torque $d\mathbf{N}$ on a small element of a current ring about its center can be calculated from eq. (63) as

$$\begin{aligned} d\mathbf{N} &= a\epsilon(\hat{\mathbf{x}} \cos \phi + \hat{\mathbf{y}} \sin \phi) \times (I d\mathbf{l} \times \mathbf{B}) \\ &= \frac{a^2 \epsilon^2 I B'_z}{2} d\phi (\hat{\mathbf{x}} \sin \phi - \hat{\mathbf{y}} \cos \phi) (\epsilon a + z\theta \cos \phi). \end{aligned} \quad (76)$$

On integrating over ϕ and recalling eq. (56) for I , we find that $N_x = 0$ and

$$dN_y = \frac{\pi}{4} z \theta \sigma a^4 v_z B_z'^2 \epsilon^3 \Delta \epsilon \Delta z. \quad (77)$$

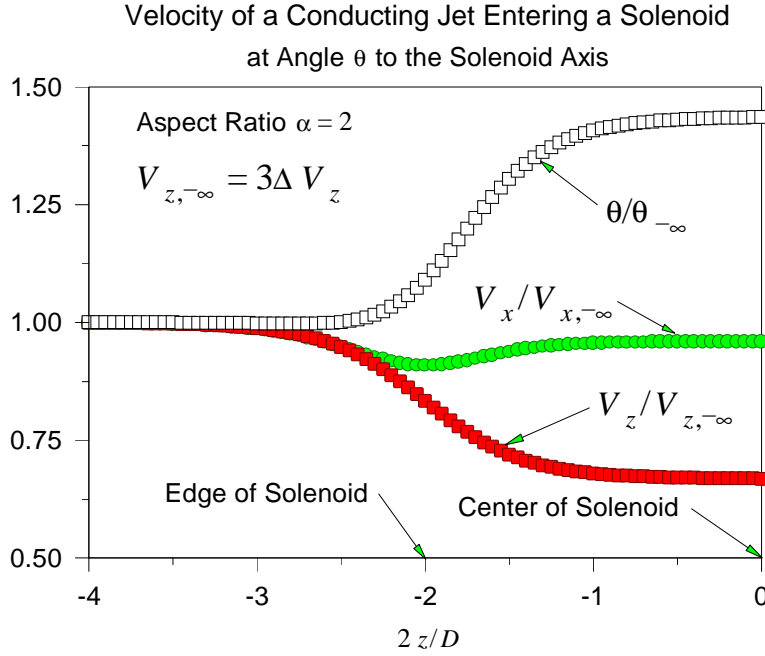


Figure 19: v_x , v_z and θ of the jet as a function of z as it enters a solenoid of aspect ratio $\alpha = 2$, according to eqs. (70-71). The initial z velocity of the jet is taken to be 3 times the loss of velocity on entering the solenoid.

The sense of rotation is to align the axis of the jet with the axis of the magnet as the jet enters the field.

Integrating over ϵ we find the total torque on a disc of radius a and thickness Δz to be

$$N_y = \frac{\pi}{16} z \theta \sigma a^4 v_z B_z'^2 \Delta z \approx \frac{x F_z}{2}. \quad (78)$$

The moment of inertia of the disc about a diameter is $ma^2/4 = \pi \rho a^4 \Delta z / 4$. Hence the angular acceleration of the azimuthal angle φ of the disc about the y axis is

$$\ddot{\varphi} = v_z \frac{d\dot{\varphi}}{dz} = \frac{\theta \sigma z B_z'^2 v_z}{4\rho}, \quad (79)$$

which is independent of the radius of the jet. Using B_z' from eq. (68), we have

$$\frac{d\dot{\varphi}}{dz} = \frac{\theta \sigma B_0^2}{4\rho D^2} \frac{z}{(1+w^2)^3}, \quad (80)$$

where as before, $w = 2z/D + \alpha$ and $\alpha = L/D$. This can be integrated once to give

$$\dot{\varphi} = v_z \frac{d\varphi}{dz} = -\frac{3\theta \sigma B_0^2}{128\rho} \left[\frac{\alpha\pi}{2} + \alpha \tan^{-1} w + \frac{\alpha w}{1+w^2} + \frac{2(1+\alpha w)}{3(1+w^2)^2} \right]. \quad (81)$$

If we ignore the variation in v_z with position, this can be integrated once more to yield

$$\varphi(z) = -\frac{3\theta \sigma B_0^2 D}{256\rho v_z} \left[\left(\alpha w + \frac{1}{3} \right) \left(\frac{\pi}{2} + \tan^{-1} w \right) + \frac{\alpha - w}{3(1+w^2)} \right]. \quad (82)$$

At the center of the magnet, $w = \alpha$, the total angle of rotation of the disc is

$$\varphi_{\text{center}} = -\frac{3\theta\sigma B_0^2 D}{256\rho v_z} \left[\left(\alpha^2 + \frac{1}{3} \right) \left(\frac{\pi}{2} + \tan^{-1} \alpha \right) \right] \approx -\frac{3\pi\alpha^2\theta\sigma B_0^2 D}{256\rho v_z}, \quad (83)$$

where the approximation holds for α somewhat larger than 1. For example, if $\alpha = L/D = 2$, $D = 0.2$ m, $B_0 = 20$ T and $v_z = 10$ m/s, we find $\varphi_{\text{center}} \approx -4\pi\theta$. With $\theta = 0.1$ rad, then $\varphi_{\text{center}} \approx -0.4\pi$.

Equation (81) indicates the interesting result that the rate of change of rotation is independent of the velocity, so the total rotation can be suppressed by increasing the jet velocity, lowering the transit time.

A liquid jet would presumably not rotate. Rather, there would be a shear, in which the portion of the jet closer to the axis is retarded more than that farther out. Our estimate that $\varphi_{\text{center}} \approx 90^\circ$ can perhaps be reinterpreted as indicating that the shear distance along the jet axis will amount to roughly the jet radius when the jet reaches the center of the magnet. This would not be troublesome.

3.3 Laboratory Observations of Eddy Currents

We have augmented our analytic results on eddy currents by observations of the motion of brass spheres, discs and rods in the field of the old Princeton cyclotron magnet, whose central field is 1 T, with a gap of 8'' between the 30''-diameter pole tips.

The spheres experienced no retarding forces due to eddy currents so long as the motion was in straight lines, whether in the uniform field region or in the fringe field. But a frictional torque opposed any rotation, even in the uniform field region.

Disks and rods experienced no drag force during steady motion in the uniform field region, but a transient drag force was experienced as the disc crossed the fringe field. Drag forces were readily observed if the trajectory of the disk was curved when in the uniform field region. Very strong frictional torques arose when the disc or rod was rotated about any axis when in the uniform field region.

We also got a negative result for the following experiment. A brass rod was slid along an aluminum V-channel, all of which was in the uniform field region. We thought that perhaps the $\mathbf{v} \times \mathbf{B}$ force on the electrons in the moving rod could generate a sideways current, which could flow in a complete circuit with the aluminum channel as the back leg. Perhaps the sliding contact was too poor to permit significant currents to flow.

Thus, we found no evidence for a ‘magnetic viscosity’ in the case of uniform motion at right angles to a uniform magnetic field. These observations are generally encouraging that a conducting jet can move through the fringe field of a solenoid magnet with only minor perturbation.

4 Measurement of Resistivities

The resistances quoted in Table 2 are probably for the alloys at room temperature, *i.e.*, solid. We have performed a simple measurement of the resistance of alloys 136 and 255 in the liquid state, using capillary tubes about 28 cm long. The inner diameters were stated

by the supplier as 0.635 mm and 1.27 mm. The tube were bent into a ‘U’ of radius about 3 cm and heated in an oven to around 160°C so that they could be filled with samples of the alloys.

The resistance of the capillary tube plus leads and contacts was measured with a Keithley 626 meter. The resistance of the leads plus contacts dipped in a single pool of liquid alloy was also measured and subtracted to yield the resistance of only a tube of liquid. Converting the results to conductivities we find $\sigma_{136} = 1.35 \times 10^6$ MKS units for alloy 136, and that this value is 85% that of the conductivity measured by us at room temperature. For liquid alloy 255 our result is $\sigma_{255} = 1.31 \times 10^6$ MKS units.

Our result for alloy 136 is very similar to that in Table 2, but our result for alloy 255 shows a slightly higher conductivity.

5 Jet Velocity *vs.* Pressure

Suppose the liquid metal is stored in a tank of area A perpendicular to the flow, and the pressure is P above atmospheric. A valve lets a jet of liquid escape through an aperture of area $a \ll A$.

Then Bernoulli’s equation tells us that the flow velocity v out the aperture obeys

$$\frac{1}{2}\rho v^2 = P + \frac{1}{2}\rho V^2, \quad (84)$$

where ρ is the density of the liquid and V is the velocity of the liquid surface of area A in the tank. The equation of continuity for an incompressible liquid tells us that $av = AV$, so that

$$v = \sqrt{\frac{2P}{\rho(1 - (a/A)^2)}} \approx \sqrt{\frac{2P}{\rho}}. \quad (85)$$

The Bi-Pb alloys have density $\rho \approx 10$ g/cm³, so the jet velocity would be

$$v[\text{m/s}] \approx \sqrt{20P[\text{atm.}]}. \quad (86)$$

For example, to reach $v = 4.5$ m/s would require 1 atm. overpressure in the storage tank.

6 The Rayleigh Instability of the Jet

6.1 Zero Magnetic Field

Following earlier work by Plateau, Rayleigh [4] deduced that a cylindrical jet is unstable against perturbations of wavelength (along the jet axis) greater than the circumference of the jet. The result of the instability is the breakup of the jet into droplets, commonly seen as water exits a nozzle. The characteristic time for onset of the instability is

$$\tau = 3\sqrt{\frac{r^3\rho}{T}}, \quad (87)$$

where the jet has radius r , mass density ρ and surface tension T . The length of the jet before breakup is then $v\tau$, where v is the velocity.

An example of breakup of a 0.5-mm-diameter mercury jet has been reported by Ansley *et al.* [6], as shown in Fig. 20. See also [7, 8, 9]. The density of mercury is $\rho = 13.5 \text{ g/cm}^3$ and the surface tension is $T = 470 \text{ dyne/cm}$. Then eq. (87) gives $\tau = 0.002 \text{ s}$ for $r = 0.025 \text{ cm}$. At 40 psi, the jet velocity was $v = 5 \text{ m/s}$, so the characteristic length before breakup is predicted to be 1 cm, in good agreement with the value 1.4 cm reported by Ansley *et al.* It thus appears that Rayleigh’s formula is valid for liquid metal jets.

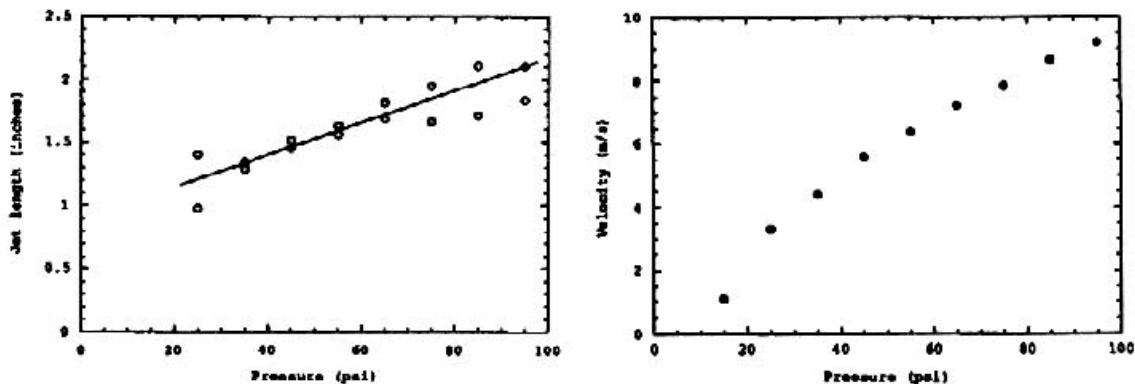


Figure 20: Length before breakup, and velocity of a mercury jet of radius 0.025 cm.

Turning to parameters relevant to the muon collider target, consider a gallium jet of radius 1 cm. The density is $\rho = 6 \text{ g/cm}^3$, and the surface tension is $T = 360 \text{ dyne/cm}$. Then the instability time is $\tau = 0.4 \text{ s}$. For a jet velocity of 10 m/s, the breakup length would be about 4 m, which is satisfactory. If the jet radius is reduced to 0.5 cm, the breakup length drops to 1.4 m.

6.2 Nonzero Axial Magnetic Field

The effect of a uniform axial magnetic field on the Rayleigh instability has been considered by Chandrasekhar [5]. There is no change in the instability time for a nonconducting liquid unless its permeability is significantly greater than 1. For a conducting liquid, Chandrasekhar introduces a quality factor,

$$Q = \frac{\mu B^2}{4\pi\eta} \sqrt{\frac{r^3}{\rho T}}, \quad (88)$$

where μ is the permeability, B is the axial magnetic field strength, and η is called the “resistivity”; I believe that $\eta = c^2/4\pi\sigma$, where σ is the electrical conductivity. For $Q > 20$, the Rayleigh instability is suppressed in the first approximation.

For mercury, $\eta = 7.5 \times 10^3 \text{ cm}^2/\text{s}$ and $Q = 1.33 \times 10^{-7} B^2 r^{3/2}$ in Gaussian units. Thus for a 20-T axial magnetic field and $r = 1 \text{ cm}$, $Q \approx 5000$, and the Rayleigh instability should be almost completely damped. This conclusion is little changed by variations in the radius

or resistivity by factors of 2, and should be valid for all liquid metal jets under consideration here.

The quality factor reaches 20 in fields slightly over 1 T (for $r = 1$ cm). Hence, unless the jet nozzle is more than a meter away from the region where the magnetic field exceeds 1 T, the Rayleigh instability will be of little concern for us.

It remains that the jet may be significantly perturbed by the nonuniform magnetic field as discussed in sec. 3, and/or by the thermal shock mentioned below.

7 Will Beam Heating Boil the Liquid Target?

If the heat from interaction of the proton beam with the liquid target boiled the target, the target might disperse violently. This would probably not have any effect on the target while the proton beam is still in it, since the time scale for this is only 1 nsec, while the time scale for dispersion is $r/v_{\text{sound}} \approx 10 \mu\text{sec}$. However, the operation of the liquid-target facility would be complicated considerably.

To estimate the magnitude of the problem we start from Fig. 4.13, p. 186 of the 1996 Muon Collider Feasibility Study. A computer simulation indicated that the power deposited in one interaction length of a mercury target by 30 Hz of pulses of 5×10^{13} 30-GeV protons would be about 750 kW. Then for a single pulse of, say, 10^{14} protons about 50 Joules/g would be deposited.

One interaction length of mercury is about 115 gm/cm^2 , so the energy deposition would be about $0.43 \text{ J-cm}^2/\text{gm}$. If we suppose this energy is deposited uniformly over radius r , which we can vary by the optics of the proton beam, then the energy deposition is

$$\frac{0.14}{[r/1 \text{ cm}]^2} \text{ J/gm.} \quad (89)$$

We haven't found any data on the boiling point of the alloys in Table 2, so we take this to be the lowest boiling point of any of the constituent elements, about 1600°C due to the bismuth. For a liquid target operating around 100°C the temperature rise to boiling is then about 1500°C . The heat capacity of the alloys will be roughly that of bismuth or lead, namely about $0.13 \text{ J}/(\text{gm}\cdot^\circ\text{C})$. Hence it will take about 200 J/gm to bring the liquid target to a boil.

Comparing with expression (89), we see that so long as

$$r > 0.025 \text{ cm,} \quad (90)$$

the liquid jet will not be brought to a boil by the proton beam.

It seems unlikely that boiling will be a problem for any realistic proton beam radius, which can then be made as small as otherwise convenient.

A small radius will permit the liquid jet velocity to be lower, as discussed in sec. 2 above.

8 Thermal Shock

While it appears that the proton beam would not boil the liquid jet, the beam does dump a lot of energy into the jet. This energy will initiate a pulse of thermal expansion that

propagates radially outward at the speed of sound – a shock wave. It is possible that this shock wave disperses the liquid into droplets, which could lead to operational difficulties.

We present a simplified model to estimate the regime in which a pressure wave might “tear” the liquid apart. When an energy ΔU (per gram) is deposited quickly in the liquid, we first calculate the temperature change ΔT that will eventually occur. Then we calculate the strain, $\Delta l/l$ corresponding to that ΔT , and evaluate the stress P corresponding to that strain. “Tearing” is likely to occur if the stress exceeds the tensile strength.

We suppose that the effective tensile strength of a liquid metal is similar to that of the same metal in solid form. For most metals, the tensile strength (pressure) P is about 0.002 of the modulus of elasticity, E (Young’s modulus). Thus,

$$\Delta U = C\Delta T = \frac{C}{\alpha} \frac{\Delta l}{l} = \frac{C}{\alpha} \frac{P}{E} \approx 0.002 \frac{C}{\alpha}, \quad (91)$$

where C is the heat capacity (J/gm-K), α is the coefficient of thermal expansion (1/K), and the approximation holds on setting the stress equal to the tensile strength. Ga-In liquid, for example, has $C \approx 0.3$ J/gm-K and $\alpha \approx 2 \times 10^{-5}$ /K. Hence, we expect the liquid will “tear” when $\Delta U \approx 30$ J/gm. This is very similar to the expected energy deposition in the muon collider target from a pulse of 10^{14} 16-GeV protons.

Indeed, experience at CERN/ISOLDE with liquid lead targets exposed to short beam pulses indicates that significant disruption of the liquid can be expected.⁴

In the future we may wish to simulate this effect using a finite-element-analysis program. Ultimately the viability of a liquid-jet target must be confirmed experimentally, preferably in a proton beam. Experiments in which an “exploding wire” is placed along the axis of a column of liquid metal may also provide useful information.

The thermal shock will be less in a material with a lower coefficient of thermal expansion. Bismuth alloys are favorable in this regard.

9 Beam-Induced Radioactivity

The high flux of protons into the target will induce some radioactivity no matter what the target consists of.

If the target contains bismuth, a sequence that results in radioactivity is:



Po²¹⁰ has a half life of 135 days and decays primarily via a 5.3-MeV α , but has a 0.1% branch to an 803-keV γ .

If, say, every beam proton results in one transmuted Bi atom, then the steady-state Po population would be equal to the total flux of protons in 135 days = $135 \times 10^5 \times 10^{15} \approx 10^{22}$ atoms, assuming a proton flux of 10^{15} /s. The number of Po decays per second would be just 10^{15} in the steady state, *i.e.*, about 30,000 Curies.

⁴*Experience with ISOLDE Molten Metal Targets at the CERN-PS Booster*, by J. Lettry *et al.*, in *Proceeding of ICANS95*.

The α -particles will be almost entirely absorbed in the target, but the 800-keV x-rays present more of a problem. The steady-state strength of the x-rays corresponds to about 30 Curies (assuming each proton results in one Po atom).

Before committing to a target containing Bi the activation of Bi by a high-energy proton beam should be studied further, both experimentally and theoretically.

A liquid target based on an In-Pb-Sn alloy (Fig. 17) might be more satisfactory from the point of view of induced radioactivity.

References

- [1] R. Palmer *et al.*, $\mu^+\mu^-$ Collider. A Feasibility Study, BNL-52503 (July, 1996),
http://puhep1.princeton.edu/~mcdonald/examples/accel/muon_collider96.pdf
- [2] R.J. Weggel, *Behavior of Conducting Solid or Liquid Jet Moving in Magnetic Field: 1) Paraxial; 2) Transverse; 3) Oblique*, BNL 65611 (June 1998),
<http://www.hep.princeton.edu/~mcdonald/mumu/target/metaljet.pdf>
- [3] J. Walker and W.M. Wells, *Drag Force on a Conductive Spherical Drop in a Nonuniform Magnetic Field*, ORNL/TM-6976 (Sept. 1979),
http://puhep1.princeton.edu/~mcdonald/examples/fluids/walker_ornl_tm6976_79.pdf
- [4] Lord Rayleigh, *The Theory of Sound* (reprinted by Dover, 1945), Vol. 2, p. 362.
- [5] S. Chandrasekhar, *Hydrodynamic and Hydromagnetic Stability* (reprinted by Dover, 1981), §112.
- [6] W.E. Ansley, S.A. Merryman and M.F. Rose, *Characteristics of Liquid Mercury Jets and the Potential Application as an Opening Switch*, Proc. Plasma Conf. **1**, 27 (1993),
http://puhep1.princeton.edu/~mcdonald/examples/fluids/ansley_ppc_1_127_93.pdf
- [7] R. Criss and M.F. Rose, *Spatial and Temporal Development of Emissions from and Exploding Mercury Jet*, IEEE Trans. Plasma Sci. **23**, 145 (1995),
http://puhep1.princeton.edu/~mcdonald/examples/fluids/criss_ieetps_23_145_95.pdf
- [8] R. Criss and M.F. Rose, *Switching and Scaling Behavior of an Exploding Mercury Jet*, Proc. Plasma Conf. **1**, 316 (1995),
http://puhep1.princeton.edu/~mcdonald/examples/fluids/criss_ppc_1_316_95.pdf
- [9] W.E. Ansley and M.F. Rose, *Evaluation of Liquid-metal Jets as the Conductor in a Rep-Rated, Exploding Fuse Opening Switch*, IEEE Trans. Magnetics **32**, 1980 (1996),
http://puhep1.princeton.edu/~mcdonald/examples/fluids/ansley_ieetm_32_1980_96.pdf